

## RESEARCH ARTICLE

10.1029/2018JD029358

## Special Section:

Winter INvestigation of  
Transport, Emissions and  
Reactivity (WINTER)

## Key Points:

- Box modeling of wintertime measurements over the eastern United States provides the first determinations of  $\phi(\text{ClNO}_2)$  yields ( $\phi(\text{ClNO}_2)$ ) from aircraft
- The median  $\phi(\text{ClNO}_2)$  value derived from the box model is overpredicted by 75–84% by the current laboratory-based  $\phi(\text{ClNO}_2)$  parameterization
- Modeled and parameterized  $\phi(\text{ClNO}_2)$  values show opposite trends with aerosol water, suggesting an incorrectly parameterized dependence

## Supporting Information:

- Supporting Information S1

## Correspondence to:

S. S. Brown and J. A. Thornton,  
steven.s.brown@noaa.gov;  
thornton@atmos.washington.edu

## Citation:

McDuffie, E. E., Fibiger, D. L., Dubé, W. P., Lopez Hilfiker, F., Lee, B. H., Jaeglé, L., et al. (2018).  $\text{ClNO}_2$  yields from aircraft measurements during the 2015 WINTER campaign and critical evaluation of the current parameterization. *Journal of Geophysical Research: Atmospheres*, 123, 12,994–13,015. <https://doi.org/10.1029/2018JD029358>



















Received 17 JUL 2018

Accepted 30 OCT 2018

Accepted article online 5 NOV 2018

Published online 25 NOV 2018

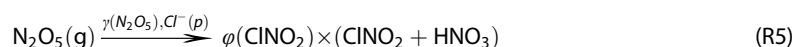
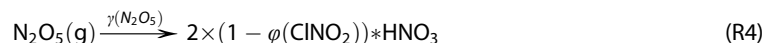
# $\text{ClNO}_2$ Yields From Aircraft Measurements During the 2015 WINTER Campaign and Critical Evaluation of the Current Parameterization

Erin E. McDuffie<sup>1,2,3</sup> , Dorothy L. Fibiger<sup>1,2,4</sup> , William P. Dubé<sup>1,2</sup>, Felipe Lopez Hilfiker<sup>5,6</sup>, Ben H. Lee<sup>5</sup> , Lyatt Jaeglé<sup>5</sup> , Hongyu Guo<sup>7</sup> , Rodney J. Weber<sup>7</sup> , J. Michael Reeves<sup>8</sup>, Andrew J. Weinheimer<sup>9</sup> , Jason C. Schroder<sup>2,3</sup> , Pedro Campuzano-Jost<sup>2,3</sup> , Jose L. Jimenez<sup>2,3</sup> , Jack E. Dibb<sup>10</sup> , Patrick Veres<sup>1,2</sup> , Carlena Ebben<sup>11</sup>, Tamara L. Sparks<sup>11</sup> , Paul J. Wooldridge<sup>11</sup>, Ronald C. Cohen<sup>11</sup> , Teresa Campos<sup>9</sup>, Samuel R. Hall<sup>7</sup> , Kirk Ullmann<sup>9</sup>, James M. Roberts<sup>1</sup> , Joel A. Thornton<sup>5</sup> , and Steven S. Brown<sup>1,3</sup> 
<sup>1</sup>Chemical Sciences Division, Earth System Research Laboratory, NOAA, Boulder, CO, USA, <sup>2</sup>Cooperative Institute for Research in Environmental Sciences, University of Colorado Boulder, Boulder, CO, USA, <sup>3</sup>Department of Chemistry, University of Colorado Boulder, Boulder, CO, USA, <sup>4</sup>Now at California Air Resources Board, Sacramento, CA, USA, <sup>5</sup>Department of Atmospheric Sciences, University of Washington, Seattle, WA, USA, <sup>6</sup>Now at TOFWERK, Thun, Switzerland, <sup>7</sup>Earth and Atmospheric Sciences Department, Georgia Institute of Technology, Atlanta, GA, USA, <sup>8</sup>Earth Observing Laboratory, NCAR, Boulder, CO, USA, <sup>9</sup>Atmospheric Chemistry Observations & Modeling Laboratory, NCAR, Boulder, CO, USA, <sup>10</sup>Institute for the Study of Earth, Oceans, and Space, University of New Hampshire, Durham, NH, USA, <sup>11</sup>Department of Chemistry, University of California Berkeley, Berkeley, CA, USA

**Abstract** Nitryl chloride ( $\text{ClNO}_2$ ) plays an important role in the budget and distribution of tropospheric oxidants, halogens, and reactive nitrogen species.  $\text{ClNO}_2$  is formed from the heterogeneous uptake and reaction of dinitrogen pentoxide ( $\text{N}_2\text{O}_5$ ) on chloride-containing aerosol, with a production yield,  $\phi(\text{ClNO}_2)$ , defined as the moles of  $\text{ClNO}_2$  produced relative to  $\text{N}_2\text{O}_5$  lost. The  $\phi(\text{ClNO}_2)$  has been increasingly incorporated into 3-D chemical models where it is parameterized based on laboratory-derived kinetics and currently accepted aqueous-phase formation mechanism. This parameterization models  $\phi(\text{ClNO}_2)$  as a function of the aerosol chloride to water molar ratio. Box model simulations of night flights during the 2015 Wintertime INvestigation of Transport, Emissions, and Reactivity (WINTER) aircraft campaign derived 3,425 individual  $\phi(\text{ClNO}_2)$  values with a median of 0.138 and range of 0.003 to 1. Comparison of the box model median to those predicted by two other field-based  $\phi(\text{ClNO}_2)$  derivation methods agreed within a factor of 1.3, within the uncertainties of each method. In contrast, the box model median was 75–84% lower than predictions from the laboratory-based parameterization (i.e., [parameterization – box model]/parameterization). An evaluation of factors influencing this difference reveals a positive dependence of  $\phi(\text{ClNO}_2)$  on aerosol water, opposite to the currently parameterized trend. Additional factors may include aqueous-phase competition reactions for the nitronium ion intermediate and/or direct  $\text{ClNO}_2$  loss mechanisms. Further laboratory studies of  $\text{ClNO}_2$  formation and the impacts of aerosol water, sulfate, organics, and  $\text{ClNO}_2$  aqueous-phase reactions are required to elucidate and quantify these processes on ambient aerosol, critical for the development of a robust  $\phi(\text{ClNO}_2)$  parameterization.

## 1. Introduction

Atmospheric reactions of nitryl chloride ( $\text{ClNO}_2$ ) contribute to tropospheric halogen activation and impact the distribution of oxidants and reactive nitrogen species in polluted regions (Simpson et al., 2015, and references therein).  $\text{ClNO}_2$  can be formed in up to a 1:1 stoichiometric ratio with soluble nitrate (particulate nitrate,  $\text{pNO}_3^-$ , or nitric acid,  $\text{HNO}_3$ ) from the heterogeneous uptake (defined as  $\gamma$ ) and subsequent reaction of dinitrogen pentoxide ( $\text{N}_2\text{O}_5$ ) ((R1)–(R5)).  $\text{ClNO}_2$  will photolyze at sunrise (R6) but can build up at night in the residual layer (RL) where the ozone ( $\text{O}_3$ ) oxidation of  $\text{NO}_x$  ( $\text{NO} + \text{NO}_2$ ) emissions forms persistent levels of  $\text{N}_2\text{O}_5$  (e.g., Brown et al., 2007; Riedel et al., 2013). The production of  $\text{ClNO}_2$  from  $\text{NO}_x$  and  $\text{O}_3$  is therefore expected to be most efficient under wintertime conditions where longer nights and cold temperatures stabilize and favor the formation of  $\text{N}_2\text{O}_5$  in its equilibrium with the nitrate radical ( $\text{NO}_3$ ) (R3) and minimize direct loss reactions of  $\text{NO}_3$  with biogenic volatile organic compounds (VOCs).



Ambient  $\text{ClNO}_2$  was first observed off the coast of Texas in 2006 (Osthoff et al., 2008). It has since been measured from ship-, ground-, and aircraft-based platforms in both continental and coastal/marine environments throughout North America (Edwards et al., 2013; Faxon et al., 2015; Kercher et al., 2009; Kim et al., 2014; Mielke et al., 2011, 2016; Osthoff et al., 2008; Riedel et al., 2012, 2013; Thornton et al., 2010; Wild et al., 2016; Young et al., 2012), Europe and the United Kingdom (Bannan et al., 2015, 2017; Phillips et al., 2012, 2016; Reyes-Villegas et al., 2018), and Asia (Liu et al., 2017; Tham et al., 2018, 2016, 2014; X. Wang, Wang, Xue, et al., 2017; T. Wang et al., 2016; Z. Wang, Wang, Tham, et al., 2017; H. Wang et al., 2018; X. Wang et al., 2014; Yun et al., 2018). Reported mixing ratios range from a few parts per trillion (pptv) to a maximum of 4,700 pptv (1-min average), measured in December 2013 in Southern China (T. Wang et al., 2016). While the absolute production of  $\text{ClNO}_2$  will depend on the rate of  $\text{N}_2\text{O}_5$  formation (R1)–(R3), the uptake efficiency of  $\text{N}_2\text{O}_5$  ( $\gamma(\text{N}_2\text{O}_5)$ ) (R4), and the presence of aerosol phase chloride (expected to vary with geographical differences in chlorine emission sources) (R5), the yield of  $\text{ClNO}_2$  relative to reacted  $\text{N}_2\text{O}_5$  ( $\phi(\text{ClNO}_2)$ ), is defined as a value between 0 and 1 and is thought to depend only on aerosol-phase chloride and water. A parameterization for  $\phi(\text{ClNO}_2)$  based on these expected dependences has been derived in previous laboratory-based studies (Behnke et al., 1997; Bertram & Thornton, 2009; Roberts et al., 2009; Ryder et al., 2015), the details of which are discussed further below. This parameterized  $\text{ClNO}_2$  production yield has been increasingly incorporated into 3-D chemical transport models in order to simulate  $\text{ClNO}_2$  formation and evaluate its tropospheric implications (e.g., Sarwar et al., 2014; Sherwen et al., 2017). Photodissociation of  $\text{ClNO}_2$  upon sunrise will release  $\text{NO}_2$  and atomic chlorine that can lead to  $\text{O}_3$  formation during the morning hours, while  $\text{HNO}_3$ , in contrast, primarily acts as a net  $\text{NO}_x$  sink in the lower atmosphere. Following this trend, a previous study with the Community Multiscale Air Quality (CMAQ) Model found up to 10% increases in 8-hr-averaged tropospheric  $\text{O}_3$  in January over the United States when including a nonzero value for  $\phi(\text{ClNO}_2)$  in the model chemical mechanism (Sarwar et al., 2014). The branching between  $\text{HNO}_3$  and  $\text{ClNO}_2$  (i.e.,  $\phi(\text{ClNO}_2)$ ) is therefore important to parameterize accurately and evaluate against field-derived results, as it has direct implications for the predicted distributions of tropospheric oxidants and  $\text{NO}_x$ .

Relatively few studies, and none from aircraft, have reported field-derived  $\text{ClNO}_2$  yields ( $\phi(\text{ClNO}_2)$ ), which require simultaneous observations of  $\text{ClNO}_2$  and additional measurements such as  $\text{N}_2\text{O}_5$  and/or total (particle + gas-phase) nitrate. Existing ground-based determinations of  $\phi(\text{ClNO}_2)$  have shown no strong seasonal or geographical dependences, and have values that vary within the entire possible range of 0 to 1 (Mielke et al., 2016; Osthoff et al., 2008; Phillips et al., 2016; Riedel et al., 2013; Tham et al., 2016, 2018; Thornton et al., 2010; Wagner et al., 2013, 2012; X. Wang, Wang, Xue, et al., 2017; H. Wang et al., 2018; Young et al., 2013; Yun et al., 2018). In addition, these field-derived  $\text{ClNO}_2$  yields are lower than those predicted by the laboratory-derived parameterization, which are based on aerosol chloride and water concentrations alone. This disagreement is found in every study that has made the comparison (Riedel et al., 2013; Ryder et al., 2015; Tham et al., 2018; Thornton et al., 2010; Wagner et al., 2013; Z. Wang, Wang, Tham, et al., 2017; X. Wang, Wang, Xue, et al., 2017), which suggests that the current mechanistic understanding of  $\text{ClNO}_2$  production may be complicated by the presence of additional aerosol-phase components or an undefined loss process that consumes  $\text{ClNO}_2$  (e.g., Roberts et al., 2008). As  $\text{ClNO}_2$  formation continues to be incorporated into 3-D models (e.g., Sherwen et al., 2017), further investigation into the source(s) of these field-model discrepancies is required to better understand and improve the predictive capabilities of  $\text{ClNO}_2$  formation in the wintertime RL.

Here we present the first aircraft determinations of  $\phi(\text{ClNO}_2)$ , derived from a box model analysis of data from the Wintertime INvestigation of Transport, Emissions, and Reactivity (WINTER) campaign, conducted over the eastern United States during 3 February to 13 March 2015. Box model  $\phi(\text{ClNO}_2)$  results are compared to other observation-based derivation methods, including the ratio of  $\text{ClNO}_2$  to total soluble nitrate, and the laboratory-based parameterization, in order to evaluate similarities and differences between methods used in previous studies. The large WINTER data set, regional coverage of WINTER flights, and multiple measurements of gas-phase species and aerosol composition additionally allow for discussion and evaluation of factors not captured by the current laboratory-based  $\phi(\text{ClNO}_2)$  parameterization. These results can help direct future laboratory studies aimed at developing a robust  $\phi(\text{ClNO}_2)$  parameterization for ambient aerosol, and in combination with our earlier work on  $\gamma(\text{N}_2\text{O}_5)$  parameterizations (McDuffie et al., 2018), can help improve model predictions of  $\text{ClNO}_2$  formation from  $\text{N}_2\text{O}_5$  heterogeneous uptake and its impact on tropospheric chemistry.

## 2. Methods

### 2.1. Measurement Campaign and Box Model

Chemical measurements, including  $\text{ClNO}_2$ , were collected aboard the National Center for Atmospheric Research/National Science Foundation (NCAR/NSF) C-130 aircraft as part of the WINTER campaign during February–March 2015 (Fibiger et al., 2018; Guo et al., 2016; Kenagy et al., 2018; Lee et al., 2018; McDuffie et al., 2018; Schroder et al., 2018). A series of 13 research flights (RFs) sampled both continental and marine environments as shown in Figure 1a, with 9 flights that included some nighttime hours. A box model, previously described by McDuffie et al. (2018), was used to simultaneously derive the production rate constant of  $\text{ClNO}_2$  ( $k_{\text{ClNO}_2}$  [ $\text{s}^{-1}$ ] =  $k_5$ ) and the total heterogeneous loss rate constant of  $\text{N}_2\text{O}_5$  ( $k_{\text{N}_2\text{O}_5}$  [ $\text{s}^{-1}$ ] =  $k_4 + k_5$ ) to calculate  $\phi(\text{ClNO}_2)$  following the  $\frac{k_5}{k_4 + k_5}$  term in equation (1). Assuming that  $\text{ClNO}_2$  is exclusively formed from reaction on aerosol particles and that it has no nighttime losses, this definition is equivalent to the rightmost term of (1) where  $\phi(\text{ClNO}_2)$  is defined as the moles of  $\text{ClNO}_2$  formed relative to the integrated moles of  $\text{N}_2\text{O}_5$  lost to aerosol uptake.

$$\phi(\text{ClNO}_2) = \frac{k_{\text{ClNO}_2}}{k_{\text{N}_2\text{O}_5}} = \frac{k_5}{k_4 + k_5} = \frac{[\text{ClNO}_2]}{\int_{\text{Sunset}}^t (k_4 + k_5)[\text{N}_2\text{O}_5] dt} \quad (1)$$

Extensive model details are presented in McDuffie et al. (2018) and are only briefly described here and in sections S1 and S2 of the supporting information. The 14-reaction chemical mechanism was initialized at 1.3 hrs prior to sunset (as determined in McDuffie et al., 2018) and integrated forward in time to simulate the nocturnal evolution of an air parcel from the onset of nocturnal chemistry (near sunset), until the time of aircraft measurement. All simulations assumed constant temperature and relative humidity (RH). Initial concentrations of  $\text{O}_3$  and  $\text{NO}_2$  were first derived by iteratively fitting the model output to reproduce 10-s-averaged observations of  $\text{O}_3$  and  $\text{NO}_2$ . Holding these initial concentrations constant,  $k_{\text{N}_2\text{O}_5}$  and  $k_{\text{ClNO}_2}$  were then adjusted to simultaneously reproduce 10-s-averaged observations of  $\text{N}_2\text{O}_5$  and  $\text{ClNO}_2$ . Finally, values of  $\phi(\text{ClNO}_2)$  (values of  $\gamma(\text{N}_2\text{O}_5)$  discussed in McDuffie et al., 2018) were calculated from the derived  $k_{\text{N}_2\text{O}_5}$  and  $k_{\text{ClNO}_2}$  products using the middle term of (1). This entire process was repeated for all points in each RF during times when the aircraft was within the RL (defined by flight based on aircraft vertical profiles of potential temperature) and the solar zenith angle (SZA) was  $>90^\circ$ . The data were averaged over 10 s to reduce variability in the data products, while maintaining the spatial resolution of  $\sim 1$  km. Minor model updates from McDuffie et al. (2018) are detailed in section S1 and minimally ( $<3\%$ ) impact both  $\gamma(\text{N}_2\text{O}_5)$  and  $\phi(\text{ClNO}_2)$  results.

Chemical measurements are briefly described here with a complete list of chemical measurements presented in Table 1 of McDuffie et al. (2018). During WINTER, multiple instruments reported 1-Hz measurements of  $\text{NO}_2$  and  $\text{O}_3$ , including the National Oceanic and Atmospheric Administration (NOAA) cavity ring down spectrometer (CRD) (Fuchs et al., 2009; Washenfelter et al., 2011), University of California Berkeley Thermal Dissociation Laser Induced Fluorescence (TD-LIF) instrument (Day et al., 2002), and the NCAR Chemiluminescence (CL) detector (Weinheimer et al., 1994). Measurement accuracies for all instruments were better than 10% for  $\text{NO}_2$  and 5% for  $\text{O}_3$ .  $\text{N}_2\text{O}_5$  was measured at 1 Hz by both the NOAA CRD (Dubé et al., 2006; Wagner et al., 2011) and the University of Washington (UW) Iodide Time-of-Flight Chemical Ionization Mass

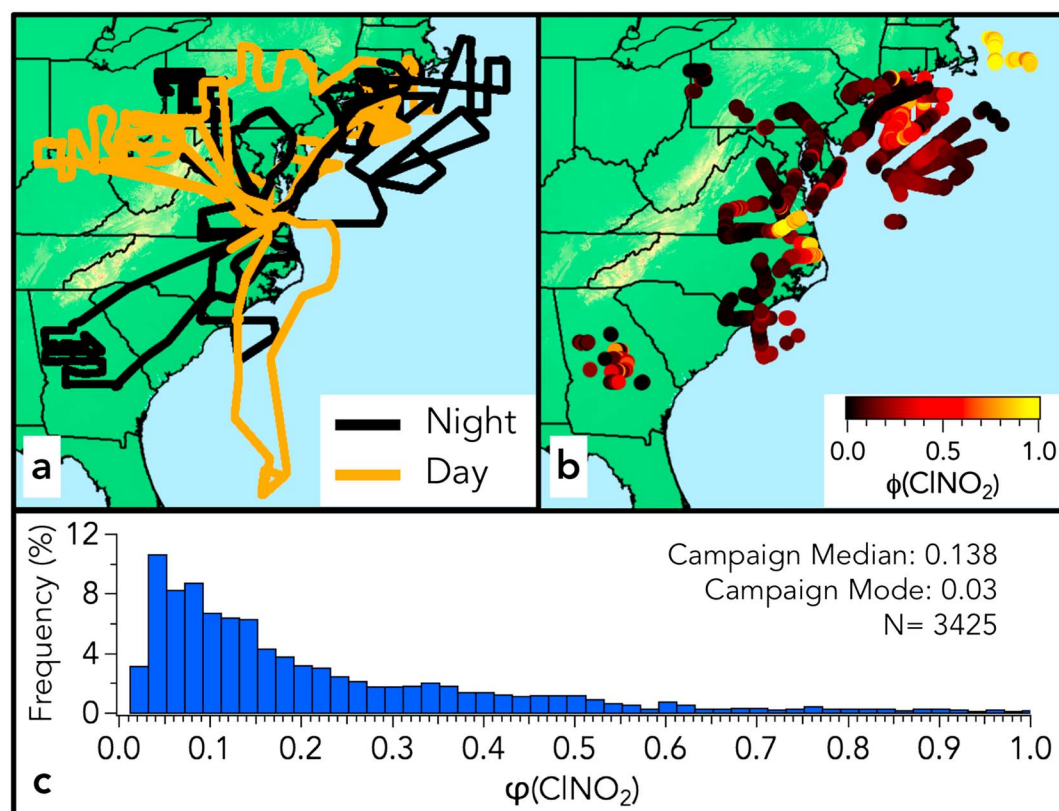


**Figure 1.** WINTER  $\phi(\text{ClNO}_2)$  box model results. (a) WINTER flight tracks colored by night ( $\text{SZA} > 90^\circ$ ) and daytime ( $\text{SZA} < 90^\circ$ ) flights. (b) WINTER flight tracks colored by 3,425 box-model-derived values of  $\phi(\text{ClNO}_2)$ . (c) Histogram of WINTER  $\phi(\text{ClNO}_2)$  results. Both are defined in the text.

Spectrometer (I-ToF-CIMS; Lee et al., 2014). Both  $\text{N}_2\text{O}_5$  measurements agreed to within their combined measurement uncertainty of 32% on all but one flight (discussed further below). Specific instruments used for WINTER simulations varied by flight, as given in the supporting information of McDuffie et al. (2018).  $\text{ClNO}_2$  was exclusively measured with the UW I-ToF-CIMS with an accuracy better than 30% and a lower limit of detection (LOD) of 0.6 pptv. Aerosol components for particles  $< 1 \mu\text{m}$  in diameter were measured by the University of Colorado Boulder High-Resolution Time-of-Flight Aerosol Mass Spectrometer (HR-ToF-AMS, hereafter referred to as AMS) (DeCarlo et al., 2006; Schroder et al., 2018) and the Georgia Institute of Technology Particle Into Liquid Sampler-coupled to Ion Chromatography (PILS-IC, hereafter referred to as PILS) (Guo et al., 2016). Detection limits (at 1 Hz) for the AMS were flight and compound dependent, typically between 0.012 and 0.474  $\mu\text{g}/\text{sm}^3$  ( $\text{sm}^3$  refers to  $\text{m}^3$  under standard conditions [1 atm and 273.15 K]), and always  $< 1.2 \mu\text{g}/\text{sm}^3$  with measurement accuracies ( $2\sigma$ ) of 35% for sulfate, nitrate, and chloride. The PILS measurements of these same compounds had accuracies of 20% with compound specific detection limits of 0.06, 0.12, 0.05  $\mu\text{g}/\text{sm}^3$  for sulfate, chloride, and nitrate, respectively. In addition, PILS data, collected for  $\sim 90$  s every 5 min, were interpolated to match the 10-s interval of the box model results. As discussed further in section 4, particulate chloride was measured by both the AMS and PILS, both of which are used in the analyses below. In contrast to the PILS, the AMS does not efficiently sample refractory species such as NaCl (Hayes et al., 2013), and the reported chloride values from the AMS are therefore expected to be lower than the PILS. Both measurements, however, reported particulate chloride concentrations during WINTER that were lower than the instrument detection limits (PILS: 0.12  $\mu\text{g}/\text{sm}^3$ , AMS: typically  $\leq 0.03 \mu\text{g}/\text{sm}^3$  for 10-s-averaged data and up to 0.05  $\mu\text{g}/\text{sm}^3$  for data points with box model results). For completeness, data reported both above and below the detection limits of each instrument are presented in the analyses below.

Aerosol water concentrations were derived as described previously in the supporting information of McDuffie et al. (2018), with an accuracy of  $\sim 25\%$ . Briefly, inorganic-associated aerosol water ( $< 1\text{-}\mu\text{m}$  diameter) was calculated using the ISORROPIA thermodynamic model (Fountoukis & Nenes, 2007) as



described in Guo et al. (2016), while the organic-associated water was estimated using a constant hygroscopicity factor of 0.1 and organic mass measured by the AMS. Data were filtered to only include points with ambient RH < 95% due to an increased uncertainty in the hygroscopic growth factor at high RH. Data were not filtered for low ambient RH, though points with <40% RH may have an increased uncertainty greater than 25% (Guo et al., 2016). The box model calculation of  $\phi(\text{ClNO}_2)$  is independent of particulate phase chloride and water and is, therefore, not subject to increased uncertainty associated with these low values. In contrast, the  $\phi(\text{ClNO}_2)$  parameterization (section 4) is sensitive to uncertainties in both particulate chloride measurements and aerosol water calculations, which are addressed in section 4.2.

## 2.2. Box Model Limitations, Uncertainties, and Sensitivity Studies

Box model results for  $\phi(\text{ClNO}_2)$  are dependent on  $k_{\text{N}_2\text{O}_5}$  and therefore subject to many of the same model limitations discussed previously in McDuffie et al. (2018). These include the assumption of constant RH and temperature during the course of an air parcel trajectory, and uncertainties in  $\text{NO}_3$  reactivity ( $k_{\text{NO}_3}$ ) (e.g., VOC measurements, direct  $\text{NO}_3$  loss, and reaction with radicals, discussed in section S2.2.5). These uncertainties can increase variability in  $k_{\text{N}_2\text{O}_5}$  and therefore in  $k_{\text{ClNO}_2}$ . Additional uncertainties specific to  $k_{\text{ClNO}_2}$  and  $\phi(\text{ClNO}_2)$  are discussed below and in detail in supporting information sections S2.1 and S2.2.

First, large measured mixing ratios of  $\text{ClNO}_2$  relative to  $\text{N}_2\text{O}_5$  can result in model non-convergence, similar to the  $\gamma(\text{N}_2\text{O}_5)$  measurement sensitivities discussed in McDuffie et al. (2018). Non-convergence occurs when values of  $k_{\text{ClNO}_2}$  equal to  $k_{\text{N}_2\text{O}_5}$  (i.e.,  $\phi(\text{ClNO}_2) = 1$ , its upper limit) are not sufficient to reproduce the observed  $\text{ClNO}_2$  mixing ratios. A total of 12.6% of WINTER points did not converge, and were removed from this analysis. The majority of these points (389 of 486 total points) occurred during RF03 in a plume of urban outflow off the coast of New York City. Model non-convergence for this and simulations of other flights could arise from multiple sources of box model uncertainties including air age (estimated from observed  $\text{NO}_x/\text{NO}_y$  ratio, as described in McDuffie et al. (2018)), simulation start time, air parcel dilution/mixing, and disagreement between the CRD and I-ToF-CIMS measurements of  $\text{N}_2\text{O}_5$ , used as a model fit parameter. Additional sensitivity tests for RF03 were performed to assess the possible sources of this model non-convergence (described in section S2.1 and Figure S1). Based on 19 sensitivity tests (section S2.1), the cause of non-convergence could not be identified. Non-convergent points, however, are not further considered in this analysis as setting each corresponding  $\phi(\text{ClNO}_2)$  to a value of 1 only increases the WINTER median by 22.8%, to a value of 0.169.

Second, model simulations were conducted assuming no interaction with the surface through dry deposition and/or surface emission. While this is a reasonable assumption for isolated air in the continental RL, a well-mixed marine boundary layer is expected at depths of at least 500 m during wintertime off the U.S. East Coast (Seidel et al., 2012). If air sampled during WINTER was in contact with the ocean surface, deposition should be included in the model. Due to uncertainties in depositional fluxes, deposition was not included in base case simulations and was instead tested through two sensitivity studies. For these tests, the depositional flux for  $\text{N}_2\text{O}_5$  was estimated using the exchange velocity derived from an observational analysis by Kim et al. (2014) (further details in section S2.2.1). Including  $\text{N}_2\text{O}_5$  deposition increased the median  $\phi(\text{ClNO}_2)$  over the ocean by 28%, from a value of 0.145 to 0.186 (ocean data only, see section S2.2.1 and Figure S2). The second test included estimates for both  $\text{N}_2\text{O}_5$  and  $\text{ClNO}_2$  deposition. While  $\text{N}_2\text{O}_5$  uptake to chloride-rich seawater is expected to result in a positive  $\text{ClNO}_2$  flux from the ocean surface (provided  $\text{ClNO}_2$  re-volatilizes to the gas phase), Kim et al. (2014) observed a slight negative  $\text{ClNO}_2$  flux from eddy covariance measurements at night at a coastal location in Southern California. Including a  $\text{ClNO}_2$  dry deposition velocity approximately one third the magnitude of that for  $\text{N}_2\text{O}_5$  (based on Kim et al., 2014) further increased the median box model  $\phi(\text{ClNO}_2)$  value over the ocean by an additional 35%, to a value of 0.251 (section S2.2.1). Both values, however, remained lower than those predicted by the laboratory-based parameterization (Figure S3), indicating that the model assumptions related to ocean exchange do not change the main conclusions presented below.

Finally, to test the overall model sensitivity to uncertainties in model fit parameters and assumptions, a series of 18 sensitivity studies were conducted for each flight, with the results presented in section S2.2 (Figures S2–S11) and summarized in Table S1. Of the parameters tested,  $\phi(\text{ClNO}_2)$  was most sensitive to uncertainties in  $\text{ClNO}_2$  and  $\text{N}_2\text{O}_5$  deposition, which increased the median  $\phi(\text{ClNO}_2)$  value over the ocean by 73%, to a value of

0.251 (discussed above). The second largest sensitivity was to assumptions in air age, with a 43.7% increase and 25.3% decrease in the median  $\phi(\text{ClNO}_2)$  under assumptions of younger and older air, respectively (Table S1 and Figure S4). Uncertainties in chemical measurements used as model fit parameters resulted in a range of  $-29.8\%$  to  $+34.5\%$  for changes in median  $\phi(\text{ClNO}_2)$  (absolute values of 0.092 to 0.164; Figures S5–S8). Data over the ocean were additionally tested for sensitivities to air parcel dilution with simultaneous entrainment of background  $\text{O}_3$ , which increased the median of this subset of points by 21.3%, from a value of 0.188 to 0.228 (Figure S2). Dilution/mixing was modeled in this test as a first order loss process for all species with a dilution rate constant of  $3.1 \times 10^{-5} \text{ s}^{-1}$ , estimated from multiple encounters of the same air parcel on RF03. An additional modeling analysis of WINTER data by Kenagy et al. (2018) derived a similar lifetime for loss associated with both mixing ( $1/\tau_{\text{mix}} = 1.9 \times 10^{-5} \text{ s}^{-1}$ ) and deposition ( $1/\tau_{\text{HNO}_3} = 1.4 \times 10^{-5} \text{ s}^{-1}$ ). The median  $\phi(\text{ClNO}_2)$  had less than 7% sensitivities in all remaining tests, including uncertainties in the time elapsed before sunset (Figure S9),  $\text{NO}_3$  reactivity (Figure S10), and photolysis rates (section S2.2.6 and Figure S11; Madronich et al., 1998; Shetter & Muller, 1999). Despite the relatively large sensitivities observed in some tests, median  $\phi(\text{ClNO}_2)$  values always remained less than 0.251, within 0.113 of the base case median and lower than the median predicted by the laboratory-based parameterization, discussed in section 4.

### 3. Results

#### 3.1. Box Model Analysis

Box model simulations resulted in 3,425 individual determinations of  $\phi(\text{ClNO}_2)$ , encompassing nearly the entire possible range, with values from 0.003 to 1. The number of  $\phi(\text{ClNO}_2)$  determinations reported here ( $N = 3,425$ ) is larger than the number of  $\gamma(\text{N}_2\text{O}_5)$  determinations reported by McDuffie et al. (2018;  $N = 2,876$ ) due to the dependence of  $\gamma(\text{N}_2\text{O}_5)$  on aerosol surface area measurements, which were not required for  $\phi(\text{ClNO}_2)$  and not always available during WINTER flights. WINTER flight tracks are colored by  $\phi(\text{ClNO}_2)$  determinations in Figure 1b, with the campaign distribution shown in Figure 1c. The  $\phi(\text{ClNO}_2)$  distribution had a median and mode of 0.138 ( $1\sigma$ :  $+0.051/-0.045$ , described below) and 0.030, respectively. Data in Figure 1b show several areas of larger  $\phi(\text{ClNO}_2)$  associated with specific flights and generally higher values downwind of New York City, the largest regional  $\text{NO}_x$  source. The  $\phi(\text{ClNO}_2)$  values otherwise do not show a strong geographical distribution. Data sampled over both ocean ( $N = 1,896$ ) and land ( $N = 1,529$ ) encompassed the same range in  $\phi(\text{ClNO}_2)$  (Figure S13), but with medians of 0.203 and 0.075, respectively. While larger yields may be expected in chloride-rich oceanic air, the two populations may be similar as many WINTER flights over the ocean sampled continental urban outflow. Box model uncertainties ( $1\sigma$ ) (time series in Figure S12) were calculated for each individual  $\phi(\text{ClNO}_2)$  value from the quadrature addition of measurement uncertainties ( $\text{O}_3$ ,  $\text{NO}_2$ ,  $\text{N}_2\text{O}_5$ , and  $\text{ClNO}_2$ ) and model sensitivities to air age, simulation start time, photolysis rates, dilution, and 50% changes in total  $k_{\text{NO}_3}$  (section S2). Sensitivity to deposition was not included in the total error calculation due to deposition rate uncertainties, but is discussed further in section 4.3.3.

WINTER values are compared in Figure 2 (and Table S2) to all previously reported field determinations of  $\phi(\text{ClNO}_2)$ . Figure 2 shows that  $\phi(\text{ClNO}_2)$  values are variable and do not show a consistent dependence on geographical location, although the current database may be too sparse to illustrate such differences on continental or regional scales. The WINTER distribution and median appear similar to those reported from both continental and coastal locations across North America (Mielke et al., 2011, 2013, 2016; Osthoff et al., 2008; Riedel et al., 2013; Thornton et al., 2010; Wagner et al., 2012, 2013; Table S2). The reported average values in Europe (Phillips et al., 2016) and polluted regions in China (Tham et al., 2016, 2018; X. Wang, Wang, Xue, et al., 2017; Z. Wang, Wang, Tham, et al., 2017; H. Wang et al., 2018; Yun et al., 2018), however, are larger than the median (Figure 2) and mean (Table S2) during WINTER.

Additional, real geographical differences in  $\phi(\text{ClNO}_2)$  may be obscured by varying  $\phi(\text{ClNO}_2)$  derivation methods used in past literature. For example, the method employed by Mielke et al. (2016), Mielke et al. (2013), and Osthoff et al. (2008) (applied to WINTER data as Method 1 in section 3.2) defines  $\phi(\text{ClNO}_2)$  as the amount of  $\text{ClNO}_2$  produced relative to the integrated amount of  $\text{NO}_3$  radical formed, not  $\text{N}_2\text{O}_5$  lost, which may be considered a lower limit to  $\phi(\text{ClNO}_2)$ . Methods relating the amount of observed  $\text{ClNO}_2$  to total nitrate, as employed by Riedel et al. (2013), Wagner et al. (2012), Phillips et al. (2016), and Tham et al. (2018) (Method #2 in section 3.2) have additional uncertainties described in the following section. Studies by Tham et al.

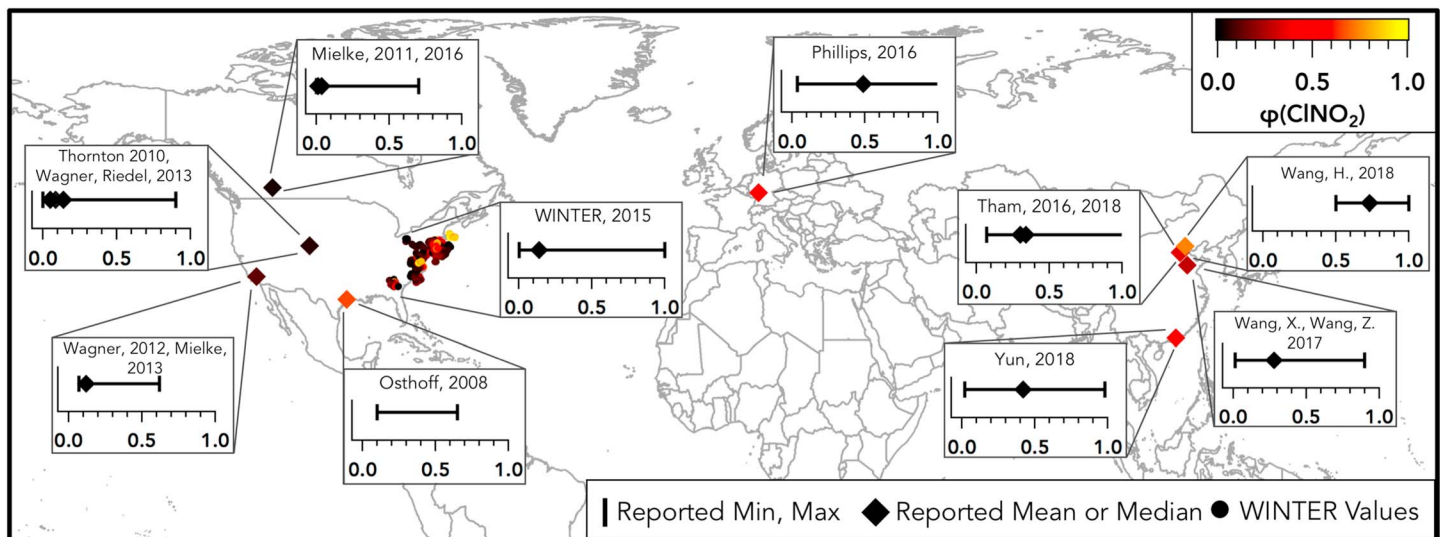


**Figure 2.** Map of all reported field determinations of  $\phi(\text{CINO}_2)$ . The geographic location of each field study is represented by a diamond, colored by the reported (or calculated) average or median value of  $\phi(\text{CINO}_2)$ , at each location. All 3,425 determinations from WINTER are shown and colored by the box-model calculated  $\phi(\text{CINO}_2)$  values. Additional graph inserts show the maximum range and median or average value reported by each study at each location.

(2014), X. Wang, Wang, Xue, et al. (2017), and Z. Wang, Wang, Tham, et al. (2017) defined  $\phi(\text{CINO}_2)$  following the right hand side of (1), equivalent to the box model calculation for WINTER, but calculated  $k_{\text{N}_2\text{O}_5}$  from the steady state approximation, which may lead to an over-prediction of  $k_{\text{N}_2\text{O}_5}$  (underprediction of  $\phi(\text{CINO}_2)$ ) in cold and/or high- $\text{NO}_x$  environments (Brown et al., 2003). The studies most directly comparable to WINTER are Yun et al. (2018) and Wagner et al. (2013), who deployed similar versions of the WINTER box model. In contrast to the WINTER model, Wagner et al. (2013) used the right side of (1) to derive  $\phi(\text{CINO}_2)$  rather than iteratively fitting the model to  $\text{CINO}_2$  observations. Further comparisons of these methods applied to WINTER data are presented next.

### 3.2. Comparison to Multiple Definitions of $\phi(\text{CINO}_2)$

In this section, four methods are applied to WINTER data in an attempt to provide a direct comparison and evaluation of methods commonly used in past literature. Due to the difference in aircraft and ground-based observational data,  $\phi(\text{CINO}_2)$  derivations using steady state-derived  $k_{\text{N}_2\text{O}_5}$  in (1) (used by Tham et al., 2016; X. Wang, Wang, Xue, et al., 2017; Z. Wang, Wang, Tham, et al., 2017) and the ratio of  $\text{CINO}_2$  to  $\text{pNO}_3^-$  production rates (used by Wang et al., 2018) could not be compared to box model results. Each additional method tested here is described below and assumes that heterogeneous production is the only source of  $\text{CINO}_2$ , and that  $\text{CINO}_2$  is stable overnight.

In Method 1,  $\phi(\text{CINO}_2)$  is defined in (2) as the amount of observed  $\text{CINO}_2$  per amount of  $\text{NO}_3$  radical produced.  $P_{\text{NO}_3}$  is defined in (3) as the instantaneous rate of nitrate radical production from the oxidation of  $\text{NO}_2$  with  $\text{O}_3$  (R2). The term  $\text{dt}_{\text{Sunset}}$  is the amount of time elapsed between the onset of nocturnal chemistry (approximately sunset) and the time of aircraft measurement. Previously used by Osthoff et al. (2008), Mielke et al. (2013), and Mielke et al. (2016), this definition of  $\phi(\text{CINO}_2)$  may be a lower limit to  $\phi(\text{CINO}_2)$  as  $\text{NO}_3$  production does not always lead to  $\text{N}_2\text{O}_5$  and subsequent  $\text{HNO}_3/\text{CINO}_2$  formation. Instantaneous  $P_{\text{NO}_3}$ , however, also decreases overnight as  $\text{NO}_2$  and  $\text{O}_3$  are consumed, which could alternatively lead to an overprediction of  $\phi(\text{CINO}_2)$  that would increase with simulation duration.

$$\phi(\text{CINO}_2) = \frac{[\text{CINO}_2]}{P_{\text{NO}_3} * \text{dt}_{\text{Sunset}}} \quad (2)$$

$$P_{\text{NO}_3} = k_2[\text{O}_3][\text{NO}_2] \quad (3)$$

Method 2 defines  $\phi(\text{CINO}_2)$  in (4), calculated from the slope of the linear regression between observed  $\text{CINO}_2$  and total soluble nitrate ( $\text{HNO}_3$  + particulate nitrate). This method has been used by Riedel et al. (2013), Wagner et al. (2012), Phillips et al. (2016), and Tham et al. (2018). Here  $\text{CINO}_2$  yields were

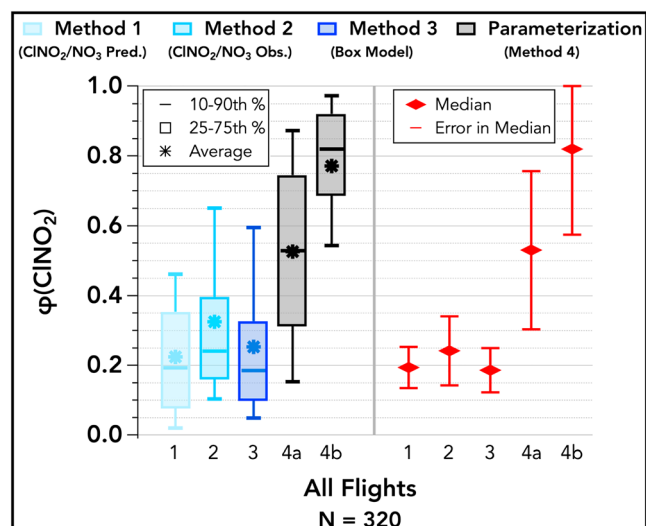


**Figure 3.** (left) Box and whisker plots comparing four derivation methods for  $\phi(\text{CINO}_2)$  during WINTER, illustrating the agreement in  $\phi(\text{CINO}_2)$  variability predicted by each method. Details of each method are described in the text and shown in the legend above. Method 4 calculates  $\phi(\text{CINO}_2)$  from the laboratory-based parameterization using both (4a) AMS and (4b) PILS particle chloride measurements. Bars represent the 10th, 50th, and 90th percentiles. Boxes show the 25th to 75th percentiles, and stars represent the averages. (right) Median values for each method are shown by red diamonds with red bars representing the uncertainty in the median for each method. Data in both panels are filtered to include points ( $N = 320$ ) where  $\phi(\text{CINO}_2)$  values were simultaneously derived for all methods.

calculated every 10 s from linear fits of 1-Hz  $\text{CINO}_2$  observations against the sum of gas-phase  $\text{HNO}_3$  and submicron particulate  $\text{NO}_3^-$  (i.e., total soluble nitrate), as measured with the I-ToF-CIMS and AMS, respectively. In these fits, intercepts were not forced to zero. Example individual correlations derived from five different flights are highlighted in Figure S14. The total number of derived fits was additionally filtered to only include individual fits with at least eight data points and statistically significant ( $p < 0.05$ ) correlation coefficients. This correlation filter is expected to bias the campaign median  $\phi(\text{CINO}_2)$  value high due to low correlations associated with many of the low  $\text{CINO}_2$  yields. Filtering all four methods for the same points, however (described below), can provide a direct methods comparison for this subset of points. Method 2 also excludes particulate  $\text{NO}_3^-$  from super micron aerosol (1–4  $\mu\text{m}$ ) due to the low measurement frequency ( $\sim 7$  min between samples), which could bias the  $\phi(\text{CINO}_2)$  values high if these large particles serve as a reservoir for nitrate formed overnight. This method also assumes no  $p\text{NO}_3^-$  contribution from reaction of  $\text{NO}_3$  with hydrocarbons, though these reactions are expected to be small due to low total  $\text{NO}_3$  reactivity during winter. To test the sensitivity of Method 2 to time-dependent processes (e.g., deposition), yields were additionally calculated from  $\text{CINO}_2$  and total nitrate correlations over increased time intervals of 30 and 100 s. At these lower time resolutions, however, the median  $\phi(\text{CINO}_2)$  changed by less than 0.06 for all three calculated intervals (10, 30, and 100 s) and number of simultaneous determinations from Methods 1–3 was reduced from 320 (described below) to fewer than 200. In comparison, the box model (Method 3) is largely independent of observed total  $\text{NO}_3^-$  and is not highly sensitive to assumptions of  $\text{NO}_3^-$  loss or previous day production.

$$\phi(\text{CINO}_2) = \frac{2m}{m+1}, \quad m = \frac{\Delta\text{CINO}_2}{\Delta(\text{HNO}_{3(g)} + \text{NO}_3^-(p))} \quad (4)$$

Method 3 is the previously described box model, while the fourth calculates  $\phi(\text{CINO}_2)$  using the laboratory-based parameterization provided in (5), using aerosol water and chloride concentrations. This particular calculation uses rate coefficient ratios from Bertram and Thornton (2009), with additional rate constant ratios discussed in the following section. Here parameterized  $\phi(\text{CINO}_2)$  values are calculated separately using measurements of particle-phase chloride from both the AMS (nonrefractory submicron chloride only) and PILS (total submicron soluble chloride) instruments, as discussed further below.

$$\phi(\text{CINO}_2) = \frac{\Delta[\text{CINO}_2]}{-\Delta[\text{N}_2\text{O}_5]} = \frac{1}{\left(1 + \frac{k_{11}[\text{H}_2\text{O}]}{k_{12}[\text{Cl}^-]}\right)} \quad (5)$$

The WINTER  $\phi(\text{CINO}_2)$  values from Methods 1–4 are compared in Figure 3. Figure 3 is not representative of the entire WINTER campaign distribution. Data have been filtered to only include points with simultaneous  $\phi(\text{CINO}_2)$  determinations from all four methods, which reduced the total number from 3,425 to 320, mostly as a result of Method 2 (ratio method). Method 2 produced the lowest number of  $\phi(\text{CINO}_2)$  determinations due to the  $r^2$  filter that required a statistically significant correlation between total nitrate and  $\text{CINO}_2$  over each 10-s interval (described above). The left panel of Figure 3 shows the 10th, 25th, 50th, 75th, and 90th percentiles, while the right shows the medians and error bars that represent the absolute  $1\sigma$  uncertainty in the median of each method (detailed in section S3.1). Briefly, the total errors associated with Methods 1 and 2 are calculated from the quadrature addition of measurement uncertainties (i.e.,  $\text{CINO}_2$ ,  $\text{O}_3$ ,  $\text{NO}_2$ ,  $\text{HNO}_3$ , and  $p\text{NO}_3^-$ ) and the absolute box model (Method 3) error is calculated as described in the previous section. Error in the parameterization (Method 4) is calculated from uncertainties in AMS and PILS chloride measurements and the aerosol water calculation.

Results in Figure 3 show that for the 320 points compared, Method 1 predicts the lowest average and percentile values (except for the 50th) for  $\phi(\text{CINO}_2)$ . The median ( $0.19 \pm (1\sigma) 0.06$ ), however, is within the



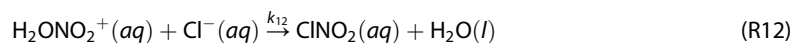
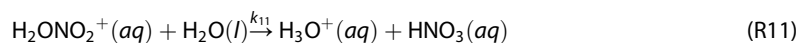
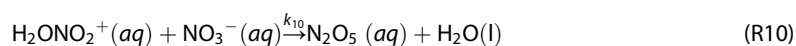
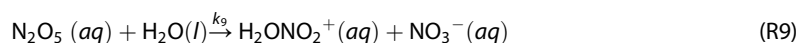
uncertainties of the medians calculated using both Methods 2 ( $0.24 \pm 0.10$ ) and 3 ( $0.19 \pm 0.06$ ) (right panel). Method 2 derived larger  $\phi(\text{ClNO}_2)$  values than Methods 1 and 3, but a median ( $0.24 \pm 0.10$ ), again, within the uncertainties of those calculated here for those methods ( $0.19 \pm 0.06$  for both) (Figure 3, right). A previous methods comparison of data from winter 2011 in Colorado also showed similarity between Methods 2 and 3, with an average  $\phi(\text{ClNO}_2)$  value of  $0.05 \pm 0.15$  using Method 2 (Riedel et al., 2013) and a mode of  $\sim 0.06$  derived from a box model similar to the one used here (Wagner et al., 2013). An additional comparison of Method 2 and the right-hand side of (1) (calculated from the steady state approach and observed  $\text{ClNO}_2$  production rates) by Z. Wang, Wang, Tham, et al. (2017) found absolute agreement within 0.03 for the campaign average  $\phi(\text{ClNO}_2)$  value at a ground site in northern China during summer 2017.

Values derived here from the parameterization in (5), using both AMS (a) and PILS (b) particle chloride measurements, were generally larger than those predicted by all other methods, with medians of 0.52 and 0.82, respectively. Larger  $\phi(\text{ClNO}_2)$  values calculated from PILS chloride data are consistent with the PILS sampling refractory chloride species. Regardless of particle chloride differences, both predicted median values that were factors of 2 to 4.3 larger than other methods, and outside the range of uncertainties associated with Methods 1 and 3 (Figure 3, right). All previous field studies to have made this comparison between data-based methods and the laboratory-based parameterization have shown an overprediction in  $\phi(\text{ClNO}_2)$  by the parameterization (Riedel et al., 2013; Tham et al., 2018; Thornton et al., 2010; Wagner et al., 2013; X. Wang, Wang, Xue, et al., 2017; Z. Wang, Wang, Tham, et al., 2017).  $\text{ClNO}_2$  yields derived from ambient seawater samples by Ryder et al. (2015) have also resulted in values lower than the parameterized equivalents. Possible factors associated with this observed difference between field-derived and parameterized  $\phi(\text{ClNO}_2)$  values during WINTER are discussed in the remaining section.

## 4. Discussion—Evaluation of the Current $\phi(\text{ClNO}_2)$ Parameterization

### 4.1. Parameterization Background

Behnke et al. (1997) first proposed the chemical mechanism for the bulk-phase reaction of aqueous  $\text{N}_2\text{O}_5$  and subsequent formation and evaporation of  $\text{ClNO}_2$ , shown in (R7)–(R13). Based on this currently accepted mechanism, an expression for  $\phi(\text{ClNO}_2)$  has been previously derived from the ratio of  $\text{ClNO}_2$  production relative to  $\text{N}_2\text{O}_5$  loss, assuming the hydrated nitronium ion intermediate ( $\text{H}_2\text{ONO}_2^+$ ) is in steady state (e.g., Bertram & Thornton, 2009). This expression, given in (5), simplifies to describe the  $\text{ClNO}_2$  yield as a competition reaction between  $\text{Cl}^-$  and  $\text{H}_2\text{O}$  for the  $\text{H}_2\text{ONO}_2^+$  intermediate (derivation reproduced in section S4). While this  $\phi(\text{ClNO}_2)$  expression has been consistent across multiple laboratory studies, kinetic laboratory experiments have reported a range of values for the  $k_{12}/k_{11}$  rate constant ratio. Based on observed  $\text{ClNO}_2$  formation from  $\text{N}_2\text{O}_5$  uptake onto aqueous NaCl particles in wetted flow tube experiments, Behnke et al. (1997) derived a value of  $836 \pm 32$  for the term  $k_{12}/k_{11}$ . More recent laboratory studies on chloride-containing aerosol have derived values in the range of 450 to 505 (Bertram & Thornton, 2009; Roberts et al., 2009; Ryder et al., 2015). These variations of the  $\phi(\text{ClNO}_2)$  parameterization are compared in Figure 4, which is described further in the following section.



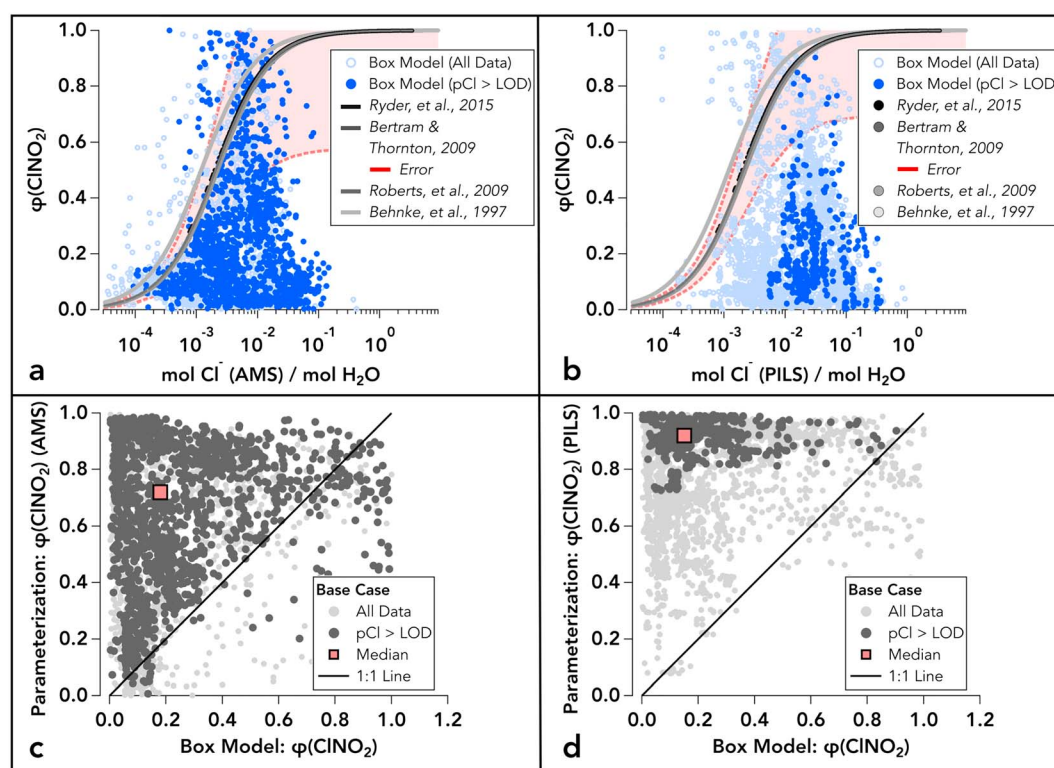


**Figure 4.** Box model results compared to parameterized  $\phi(\text{CINO}_2)$  values. (a and b)  $\phi(\text{CINO}_2)$  as a function of WINTER aerosol  $\text{Cl}^-:\text{H}_2\text{O}$  molar ratio, calculated from (a) AMS and (b) PILS particulate chloride measurements. Laboratory-based parameterizations are shown by gray lines and WINTER box model results shown by blue circles. Red dashed lines represent the total absolute upper and lower error limits of the Bertram and Thornton (2009) parameterization. (c and d) Parameterized  $\phi(\text{CINO}_2)$  values against box model results, using (c) AMS and (d) PILS chloride measurements. Black lines are the 1:1 line. In all panels, data with particulate chloride measurements above reported detection limits for AMS and PILS instruments are shown by dark circles; all remaining data are in light blue or gray. Medians are shown in (c) and (d) for data with particulate chloride above instrument detection limits.

#### 4.2. Box Model and Chemical $\phi(\text{CINO}_2)$ Parameterization Comparison

Parameterized predictions of the WINTER  $\phi(\text{CINO}_2)$  values are shown with the base case box model results in Figures 4a–4d. In Figures 4a and 4b, the parameterized  $\phi(\text{CINO}_2)$  values (gray/black lines) and the box model results (blue circles) are plotted as a function of the aerosol  $\text{Cl}^-:\text{H}_2\text{O}$  molar ratio, calculated with aerosol water estimates and particulate chloride measurements from both AMS (a) and PILS (b) instruments. Aerosol water and chloride concentrations from 1–4  $\mu\text{m}$  particles were not included in Figure 4 due to the small fractional contribution of this size range to aerosol surface area (0–2%) (required for  $\text{N}_2\text{O}_5$  uptake), relative to the total surface area contribution from smaller particles (<1  $\mu\text{m}$ ). The presence of chloride in these larger particles more likely contributes to the formation of gas-phase HCl through acid displacement, which can serve as a pool of chloride that equilibrates with submicron particles (Osthoff et al., 2008). Dark blue circles in Figures 4a and 4b indicate points where reported aerosol chloride concentrations were above the instrument detection limits. Figures 4c and 4d further show the correlations between the box model results (x axis) and parameterized  $\phi(\text{CINO}_2)$  values (y axis) using the Bertram and Thornton (2009)  $k_{12}/k_{11}$  ratio and AMS (c) and PILS (d) particulate chloride. Similarly to Figures 4a and 4b, dark gray circles in Figures 4c and 4d indicate where particulate chloride concentrations were measured above instrument detection limits, with the median  $\phi(\text{CINO}_2)$  values for these subsets shown by the red squares.

Results in Figure 4 demonstrate a  $\phi(\text{CINO}_2)$  overprediction by the parameterization (regardless of  $k_{12}/k_{11}$  ratio), which was also shown for a subset of WINTER data in the previous section. In Figure 4, over 90% of the individual box model  $\phi(\text{CINO}_2)$  values are overpredicted by the Bertram and Thornton (2009) parameterization, when calculated using both AMS and PILS aerosol chloride. In addition, the ratio of the box model

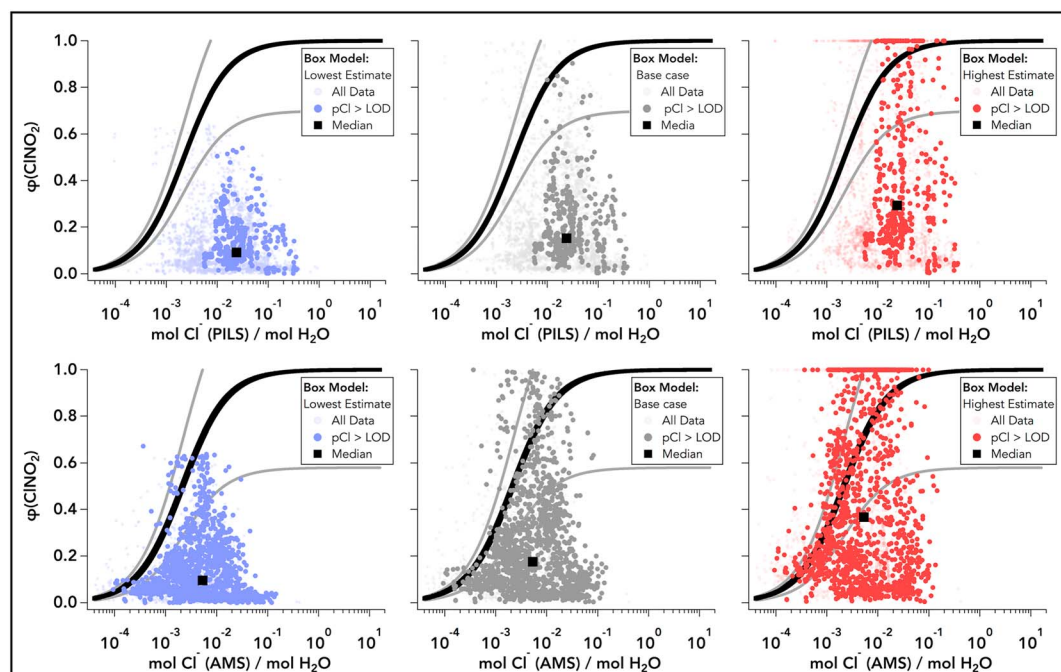


**Figure 5.** Highest (red) and lowest (blue) estimated box model  $\phi(\text{CINO}_2)$  values, plotted against WINTER  $\text{Cl}^-:\text{H}_2\text{O}$  molar ratios. Black curves represent the  $\phi(\text{CINO}_2)$  values predicted by the Bertram and Thornton (2009) parameterization. Gray curves are the upper and lower limits of the parameterization error. Squares represent the median of each set of modeled WINTER  $\phi(\text{CINO}_2)$  values ( $p\text{Cl}^- > \text{LOD}$  points only), plotted at the WINTER median  $\text{Cl}^-:\text{H}_2\text{O}$  molar ratio.

median to the medians calculated using the Bertram and Thornton (2009) parameterization range from 0.25 to 0.16, using PILS and AMS chloride, respectively. In other words, the box model median  $\phi(\text{CINO}_2)$  value is 75–84% lower than the medians calculated from the parameterization (i.e., (parameterization – box model)/parameterization).

Differences between the box model and parameterized  $\phi(\text{CINO}_2)$  values may result from uncertainties in either derivation method. To assess the role of uncertainty in the parameterization, estimates of the upper and lower limits of the parameterized values are shown by the dashed red lines in Figures 4a and 4b, calculated from the Bertram and Thornton (2009)  $k_{12}/k_{11}$  ratio and uncertainties in aerosol water (~25%) and chloride (35% AMS, 20% PILS). Both sets of chloride measurements, above and below instrument detection limits, are also included in Figure 4. Though the majority ( $\geq 50\%$ ) of reported chloride observations were below instrument detection limits (light blue [Figures 4a and 4b] and gray [Figures 4c and 4d]), over 73% of the box model  $\phi(\text{CINO}_2)$  values that corresponded to above-LOD chloride measurements, fell below the lower-limit estimate of the  $\phi(\text{CINO}_2)$  parameterization (lower red line in Figures 4a and 4b). This trend was consistent between parameterizations calculated using both AMS and PILS measurements, suggesting that uncertainties in the parameterization from the combined uncertainty in aerosol chloride and water are not responsible for the majority of overprediction by the simple chemical  $\phi(\text{CINO}_2)$  parameterization.

To further assess the contribution of box model error to the observed differences in Figure 4, upper- and lower-limit box model values (calculated from the analysis of total model error) are plotted together with parameterized  $\phi(\text{CINO}_2)$  values in Figure 5, as a function of  $\text{Cl}^-:\text{H}_2\text{O}$ , using the Bertram and Thornton (2009)  $k_{12}/k_{11}$  ratio. As discussed in section 3.1, error in each box model-derived  $\phi(\text{CINO}_2)$  value was individually calculated from the quadrature addition of measurement uncertainties ( $\text{O}_3$ ,  $\text{NO}_2$ ,  $\text{N}_2\text{O}_5$ , and  $\text{CINO}_2$ ) and model sensitivities to air age, simulation start time, dilution, photolysis rates, and 50% changes in total  $k_{\text{NO}_3}$ . Of these parameters, air age (discussed in section S2.2.1) was the largest contributor to the total model error shown in Figure S12 and Table S1. In Figure 5, points of model non-convergence during sensitivity studies (i.e.,  $k_{\text{CINO}_2} > k_{\text{N}_2\text{O}_5}$ ) were conservatively set to  $\phi(\text{CINO}_2)$  values of 1. Results show that the median box model values (black squares in Figure 5, calculated from data with particulate chloride  $> \text{LOD}$ ) remain

lower than their parameterized equivalents in all comparisons, regardless of chloride measurement. This comparison indicates that while the WINTER  $\phi(\text{ClNO}_2)$  values are sensitive to model assumptions (air age in particular), box model uncertainties are not the main source of difference between the model and laboratory-based  $\phi(\text{ClNO}_2)$  parameterization.

When considering uncertainties in each derivation method, results in Figures 4 and 5 suggest that field-derived  $\phi(\text{ClNO}_2)$  values are overpredicted by the laboratory-based parameterization. These results are qualitatively consistent with all other reported field-parameterization comparisons (Riedel et al., 2013; Ryder et al., 2015; Tham et al., 2018; Thornton et al., 2010; Wagner et al., 2013; Z. Wang, Wang, Tham, et al., 2017; X. Wang, Wang, Xue, et al., 2017), suggesting the presence of at least one physiochemical process suppressing  $\phi(\text{ClNO}_2)$  relative to production yields predicted on pure NaCl/inorganic aqueous solutions. In the following sections we use box model  $\phi(\text{ClNO}_2)$  results and observed WINTER variables to examine possible sources of the difference between the box model and the laboratory-based  $\phi(\text{ClNO}_2)$  parameterization. In the first section we discuss trends in this difference with measured aerosol components, particularly aerosol water. The last two sections assess two possible mechanistic sources of  $\phi(\text{ClNO}_2)$  suppression that have been discussed previously in field (Mielke et al., 2013; Phillips et al., 2016; Tham et al., 2018; Z. Wang, Wang, Tham, et al., 2017) and laboratory-based (e.g., Roberts et al., 2008; Ryder et al., 2015) studies of  $\text{ClNO}_2$  yield. These include: (1) the presence of additional competition reactions for the  $\text{H}_2\text{ONO}_2^+$  intermediate and (2) direct loss of gas- or aqueous-phase  $\text{ClNO}_2$  via surface deposition/aerosol uptake and aqueous-phase reaction.

### 4.3. Sources of Parameterization-Box Model Differences

#### 4.3.1. Observed Trends/Water Dependence

Of the aerosol components calculated or measured during WINTER, the difference between parameterized and box model-derived  $\phi(\text{ClNO}_2)$  values was most strongly correlated with aerosol water. Table S3 shows that the largest correlation coefficients (for both PILS and AMS calculated parameterizations) were associated with aerosol water molarity ( $r^2 = 0.54$  [AMS], 0.22 [PILS]), ambient RH ( $r^2 = 0.53$  [AMS], 0.27 [PILS]), and aerosol liquid water content (water mass fraction) ( $r^2 = 0.51$  [AMS], 0.21 [PILS]). The only other parameters with correlation coefficients above 0.1 were with wet (including aerosol water) mass fractions of aerosol organics, sulfate, and ammonium. When eliminating the role of water, the dry (excluding water) mass fractions produced lower correlation coefficients ( $r^2 \leq 0.05$ ) for each of these species. Similarly, correlations with aerosol molar ratios of  $\text{Cl}^-/\text{NO}_3^-$ , pH (from Guo et al. (2016)), and O:C ratio produced correlation coefficients less than 0.09. Two previous field studies observed a negative correlation between absolute  $\phi(\text{ClNO}_2)$  values (derived using the steady state of  $\text{N}_2\text{O}_5$ ) and aerosol-phase nitrate mass (Z. Wang, Wang, Tham, et al., 2017), as well as low  $\text{ClNO}_2/\text{N}_2\text{O}_5$  gas-phase ratios corresponding to aerosol with low  $\text{Cl}^-/\text{organic}$  mass ratios (Mielke et al., 2013). Neither of these studies quantitatively evaluated the role of aerosol composition in the difference between parameterized and field-derived values. For comparison, WINTER box model  $\phi(\text{ClNO}_2)$  values were only weakly correlated with  $\text{Cl}^-/\text{organic}$  mass ratio ( $r^2 \leq 0.027$  for both chloride measurements) and showed an even weaker, positive correlation with aerosol nitrate mass ( $r^2 = 0.024$ ).

The difference between the  $\phi(\text{ClNO}_2)$  parameterization and box model results for each individual point is plotted against aerosol water molarity in Figure 6 (for both AMS [a] and PILS [b] chloride measurements). Trends in Figure 6 show negative correlations between this difference and aerosol water for points with aerosol chloride both above and below the instrument detection limits (black and gray points, respectively). While quantitatively different slopes are derived from each fit, all trends (with AMS and PILS chloride, above and below detection limits) are qualitatively consistent, suggesting that either aerosol water or an associated factor is an important predictor of the difference between the field-derived  $\phi(\text{ClNO}_2)$  values and those predicted by the current parameterization. Based on the aqueous formation mechanism in (R7)–(R13), the role of water in the yield of  $\text{ClNO}_2$  is to act in competition with aqueous-phase chloride for the  $\text{H}_2\text{ONO}_2^+$  intermediate. This competition results in a decrease in the parameterized  $\phi(\text{ClNO}_2)$  as water increases (Figures S15a and S15b). The opposite trend is generally observed for WINTER box model results, which show a positive correlation with water (Figure S15c). Two RFs with the largest water concentrations (exceeding 40 [M]), however, showed no observable trends. Combined, these opposite trends with water lead to the negative slopes in Figure 6.



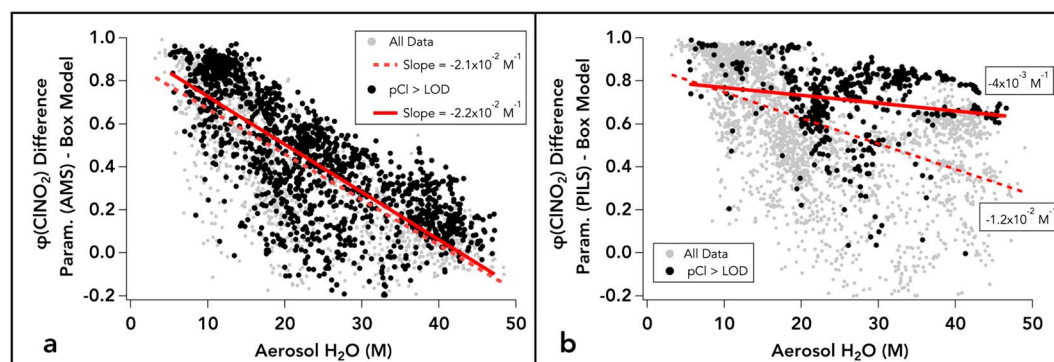


**Figure 6.** Difference between the  $\phi(\text{CINO}_2)$  parameterization and WINTER box model results, calculated using (a) AMS and (b) PILS particulate chloride. Data points above chloride detection limits (LOD) are shown in black with the fit line slopes (solid line) provided in each panel. All data points are shown in gray with fit line slopes (dashed lines) provided in each panel.

Aerosol water is a calculated rather than observed quantity, and could therefore be assumed as a potential source of the disagreement between predicted and observed trends in  $\phi(\text{CINO}_2)$ . Nevertheless, the trends in Figure 6 are unlikely the result of uncertainty in calculated water molarity. For example, points below 20-M  $\text{H}_2\text{O}$  in Figure 6 would require  $\text{H}_2\text{O}$  concentrations in (5) to be more than 100 times larger, on average, to bring the parameterization into agreement with the box model, well outside the  $\sim 25\%$  uncertainty in  $[\text{H}_2\text{O}]$ . Disagreement with the box model at low aerosol water (and RH) may, therefore, suggest that laboratory-based parameterizations are not largely applicable to environments with limited aerosol water since they have been derived from studies conducted at either high RH ( $> 55\%$ ) or on aqueous solutions (Behnke et al., 1997; Bertram & Thornton, 2009; Roberts et al., 2009; Ryder et al., 2015). Correlations between aerosol water and box model  $\phi(\text{CINO}_2)$  values in Figure S15c, however, also show quantitatively different trends for each flight, suggesting that multiple factors may be contributing to the discrepancy between box model and parameterized  $\phi(\text{CINO}_2)$  values. Only two previous field studies have examined the  $\phi(\text{CINO}_2)$  relationship with water. While  $\phi(\text{CINO}_2)$  values at a ground site in NW Germany showed no trend between RH values of  $\sim 65$  and  $90\%$  (corresponding to WINTER water concentrations of  $\sim 20$ – $45$  M) (Phillips et al., 2016), a weak positive correlation of  $\phi(\text{CINO}_2)$  with aerosol water ( $\sim 10$ – $60$  M) was also observed at a ground site in Northern China (Tham et al., 2018). Further studies of  $\text{CINO}_2$  production under a range of aerosol water conditions will be required to confirm this result.

The physical mechanism for the observed box model trend with water is uncertain but may be related to the physical availability of chloride, as discussed in previous studies as a possible cause of  $\phi(\text{CINO}_2)$  suppression in field-derived results (Mielke et al., 2013; Phillips et al., 2016; Z. Wang, Wang, Tham, et al., 2017). The current  $\phi(\text{CINO}_2)$  parameterization assumes internally mixed aerosol where all  $\text{Cl}^-$  is available for reaction, which may not be the case for ambient aerosol. For example, measured particulate chloride may not be present equally throughout the particle size distribution, an effect that would increase the parameterized  $\phi(\text{CINO}_2)$  values if the largest chloride concentrations were present in a different size range than the particles contributing most to the surface area density (i.e., participating in  $\text{N}_2\text{O}_5$  uptake). Based on the WINTER aerosol size distributions measured by the UHSAS ( $0.06$ – $1$   $\mu\text{m}$ ) and PCASP ( $1$ – $3$   $\mu\text{m}$ ), the median of the aerosol surface area distribution ( $dS/d\log D_p$ ) corresponded to particle diameters between  $0.12$  and  $0.3$   $\mu\text{m}$ , for the data shown in Figure 4. The size distribution of total particulate chloride, however, was not reported during WINTER and cannot be further evaluated as a possible source of observed difference between the  $\phi(\text{CINO}_2)$  parameterization and box model results.

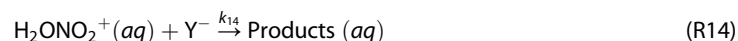
Additionally, even if particulate chloride is present evenly throughout the size distribution, it may not be accessible within the aerosol itself, which may depend on RH and the physical and chemical properties of the aerosol. For example, previous studies have found that aqueous  $\text{Cl}^-$  has a propensity to partition away from the surface (e.g., Cummings & Wick, 2013) and that submicron sea salt aerosol may form organic coatings (Ault et al., 2013), especially when aged (Laskin et al., 2012). The increased presence of aerosol organics relative to water has also been shown to change the rate of diffusion and solubility of aqueous  $\text{N}_2\text{O}_5$  (e.g., Anttila et al., 2006; Gaston et al., 2014) and, therefore, may also impact the mobility of  $\text{Cl}^-$  ions by inducing changes in

the aerosol phase or viscosity (e.g., Gržinić et al., 2015; Shiraiwa et al., 2017) and/or the formation of liquid-liquid phase separations (e.g., Bertram et al., 2011). Each of these processes is dependent on RH and the presence of organics and may serve to limit the availability of  $\text{Cl}^-$  at the aerosol surface under low aerosol water conditions. This would reduce field-derived  $\phi(\text{ClNO}_2)$  values relative to the parameterization if  $\text{N}_2\text{O}_5$  dissociation and reaction occurs near the surface, physically removed from  $\text{Cl}^-$  residing in the bulk.

Changes in aerosol phase and morphology (i.e., core-shell) associated with RH and organic content were not measured during WINTER, but a parameterization by Bertram et al. (2011) was used with RH and O:C ratio measurements to predict the presence of liquid-liquid phase separations, as described in section S3.2. Results in Figure S16, however, show that predictions of phase-separated aerosol do not consistently correspond with the largest differences between the box model results and  $\phi(\text{ClNO}_2)$  parameterization. In contrast, many of the largest  $\phi(\text{ClNO}_2)$  differences were associated with the longest organic aerosol mixing times (i.e., largest aerosol diffusion coefficients), predicted by two RH-dependent parameterizations for 200-nm diameter  $\alpha$ -pinene secondary organic aerosol (SOA), presented by Maclean et al. (2017) (shown in Figure S17). Aerosol mixing time parameterizations, however, have only been developed for  $\alpha$ -pinene SOA and still have significant uncertainty (Maclean et al., 2017) and therefore require more work to determine their applicability to low biogenic WINTER aerosol (see McDuffie et al., 2018) and the extent to which diffusion may impact  $\phi(\text{ClNO}_2)$ . As described in section S3.2, a similar parameterization for aerosol viscosity by Shiraiwa et al. (2017) could not be calculated from WINTER data. Lastly, previous studies have additionally used estimates of the  $\text{N}_2\text{O}_5$  diffusion distance prior to reaction (reacto-diffusive length), together with aerosol size and composition to predict  $\text{N}_2\text{O}_5$  uptake onto organic and inorganic aerosol (e.g., Anttila et al., 2006; Gaston et al., 2014; Gaston & Thornton, 2016). The utility of this parameter to predict changes in  $\phi(\text{ClNO}_2)$ , however, has not been previously examined and remains uncertain here as the  $\phi(\text{ClNO}_2)$  difference does not strongly correlate with relevant variables other than aerosol water, such as O:C ratio and organic content (Table S3). Therefore, while the observed water trend may be related to chloride availability, which could be impacted by organic-induced changes in aerosol morphology and viscosity, the cause of this trend remains inconclusive.

#### 4.3.2. Additional Aqueous Competition Reactions

Reaction between the  $\text{H}_2\text{ONO}_2^+$  intermediate and species other than  $\text{Cl}^-$  and  $\text{H}_2\text{O}$  could additionally contribute to the observed suppression of  $\phi(\text{ClNO}_2)$  on ambient aerosol. Such a process would add an additional competition reaction in the form of (R14) to the mechanism in (R7)–(R13). In order for a reaction of this form to compete with aqueous  $\text{Cl}^-$  and cause a reduction in  $\text{ClNO}_2$  production relative to  $\text{N}_2\text{O}_5$  uptake, the product of  $k_{14}$  and the concentration of additional reactive compounds would have to be comparable to  $k_{12}[\text{Cl}^-]$ . In addition, agreement between the box model and two nitrate-dependent observational  $\phi(\text{ClNO}_2)$  methods (Figure 3), suggests that this reaction would also have to produce particle-phase nitrate or gas-phase  $\text{HNO}_3$  to maintain consistency between the observational methods.



Previous studies have reported evidence of a competition between particle-phase chloride and halogens. For example, enhanced  $\text{Br}_2$  formation relative to  $\text{ClNO}_2$  has been observed on ice at  $\text{Cl}^-:\text{Br}^-$  ratios  $<30$  (Lopez-Hilfiker et al., 2012). In addition, reaction of  $\text{N}_2\text{O}_5$  with dilute NaI and NaBr solutions has shown production of  $\text{BrNO}_2$ ,  $\text{Br}_2$ , and  $\text{I}_2$  (e.g., Behnke et al., 1994; Schweitzer et al., 1998). While the latter studies do not show direct competition with  $\text{Cl}^-$ , the stronger nucleophilic character of  $\text{Br}^-$  and  $\text{I}^-$  relative to chloride may allow for efficient competition. Ambient  $\text{Br}^-$  and  $\text{I}^-$  concentrations in sea water (expected  $\text{Cl}^-:\text{Br}^-:\text{I}^-$  ratios of  $\sim 1:1 \times 10^{-3}:1 \times 10^{-6}$ ) may be too small, however, to compete with  $\text{Cl}^-$  via (R14) during WINTER. These species may alternatively reduce  $\phi(\text{ClNO}_2)$  via direct reaction with  $\text{ClNO}_2$ , further discussed in the following section. In addition, these reactions may not lead to the production of  $\text{NO}_3^-$  or  $\text{HNO}_3$  (e.g.,  $\text{BrNO}_2$  formation), making the presence of these reactions potentially inconsistent with the previous observation-based methods (Figure 3), which incorporate nitrate mass balance between  $\text{N}_2\text{O}_5$ , particulate nitrate,  $\text{HNO}_3$ , and  $\text{ClNO}_2$ .

Additional studies have also found efficient reaction between the nitronium ion and aqueous-phase aromatics (Hoggett et al., 1971; Lüttke et al., 1997; Schofield, 1980; Taylor, 1990). Experiments focused specifically on reactions with a subset of phenols (Heal et al., 2007) derived  $k_{14}/k'_{11}$  ratios ( $k'_{11} = k_{11}[\text{H}_2\text{O}]$ ) that

correspond to  $k_{14}/k_{11}$  ratios (for average WINTER aerosol water concentrations of 20 M) over an order of magnitude larger than the  $k_{12}/k_{11}$  ratios reported by Behnke et al., 1997; Bertram & Thornton, 2009; Roberts et al., 2009; and Ryder et al., 2015 (further details in section S5). Additionally, flow tube reactions of  $\text{N}_2\text{O}_5$  uptake onto seawater mimics (Ryder et al., 2015) showed that both phenol and humic acid at low concentrations ( $<10$  mM) could cause significant reductions in  $\phi(\text{ClNO}_2)$  relative to pure NaCl solutions, which may result from both a large  $k_{14}$  reaction rate constant and enhanced surface concentration of organics relative to chloride (Ryder et al., 2015). Combined, these past results suggest that even at low organic concentrations, additional competition reactions, generalized by (R14), could effectively compete with (R12) and decrease the  $\text{ClNO}_2$  production yield relative to that expected from  $\text{Cl}^-$  and water alone. These reactions may also lead to aerosol-phase  $\text{NO}_3^-$ , organic nitrates, or  $\text{HNO}_3$ , maintaining consistency with observational derivations. While AMS measurements of total nitrate during WINTER did show evidence for the presence of organic nitrates, the calculated *inorganic-only* nitrate (scaled to PILS-IC measurements; see Schroder et al., 2018) was consistently the largest fraction of total aerosol nitrate measured.

To examine whether there is evidence in the WINTER data to support competition reactions, an additional expression for  $\phi(\text{ClNO}_2)$  was derived from (R9)–(R12) and (R14), shown in (6), assuming the  $\text{H}_2\text{ONO}_2^+$  intermediate is in steady state (see derivation in section S4). Rearranging this expression in (7), a plot of  $(\phi(\text{ClNO}_2)^{-1} - 1) * [\text{Cl}^-]/[\text{H}_2\text{O}]$  against  $[\text{Y}^-]:[\text{H}_2\text{O}]$  should yield a linear correlation with a slope of  $k_{14}/k_{12}$  and intercept of  $k_{11}/k_{12}$ . The identity of  $\text{Y}^-$  is unknown, but it could include aqueous-phase species such as organics, halogens, and/or anions such as  $\text{SO}_4^{2-}$  that could plausibly react with  $\text{H}_2\text{ONO}_2^+$ . Previous studies on dilute  $(\text{NH}_4)_2\text{SO}_4$ ,  $(\text{NH}_4)\text{HSO}_4$ , and chloride containing solutions, however, have not shown a suppression in  $\phi(\text{ClNO}_2)$  relative to the parameterization (Roberts et al., 2009) and have indicated that at similar concentrations,  $\text{Cl}^-$  is more reactive toward  $\text{H}_2\text{ONO}_2^+$  than  $\text{SO}_4^{2-}$  (Gaston & Thornton, 2016). To maintain consistency between the box model and other observational methods, possible competition reactions would also need to produce either particle or gas-phase nitrate through, for example, hydrolysis of the initial anion-nitronium product in (R14).

$$\phi(\text{ClNO}_2) = \frac{1}{\left(1 + \frac{k_{11}[\text{H}_2\text{O}]}{k_{12}[\text{Cl}^-]} + \frac{k_{14}[\text{Y}^-]}{k_{12}[\text{Cl}^-]}\right)} \quad (6)$$

$$\left(\frac{1}{\phi(\text{ClNO}_2)} - 1\right) * \frac{[\text{Cl}^-]}{[\text{H}_2\text{O}]} = \frac{k_{11}}{k_{12}} + \frac{k_{14}[\text{Y}^-]}{k_{12}[\text{H}_2\text{O}]} \quad (7)$$

Figure 7 shows the correlation between the left term in (7) (rearranged from (6)) and molar ratios of (a)  $\text{SO}_4^{2-}:\text{H}_2\text{O}$  and (b)  $\text{Org}:\text{H}_2\text{O}$  (assuming a constant organic molecular weight of 250 g/mol). An additional correlation with the  $\text{Br}^-$  reaction product,  $\text{Br}_2$  (e.g., Behnke et al., 1994; Schweitzer et al., 1998) ( $\text{BrNO}_2$  not present above instrument LOD), measured by the I-ToF-CIMS, was not statistically significant (not shown). The fit results in Figure 7 provide mixed evidence for the presence of a competition between organics,  $\text{SO}_4^{2-}$ , and  $\text{Cl}^-$  via (R14) during WINTER. The positive correlations are consistent with competition with  $\text{Cl}^-$ , with a rate constant ( $k_{14}$ ) 1.5–50 times larger than  $k_{12}$  (Figure 7). The negative fit intercepts, however, also indicate that this model for  $\phi(\text{ClNO}_2)$  is incorrect when using  $\text{SO}_4^{2-}$  and total aerosol organics as species  $\text{Y}^-$ . It is possible, however, that the negative intercepts could result from multiple competition reactions of different rates (i.e., with various organic components) and/or additional processes that cause suppression.

Alternatively, the hypothesis of a competition reaction can be tested by fitting the  $[\text{Y}^-]:[\text{Cl}^-]$  ratio in (7) to WINTER box model  $\phi(\text{ClNO}_2)$  values. This method does not require knowledge of  $\text{Y}^-$  and estimates the  $[\text{Y}^-]:[\text{Cl}^-]$  ratio that would be required to explain the observed  $\phi(\text{ClNO}_2)$  values via (R14) by using the  $k_{11}/k_{12}$  ratio of 0.002 from Bertram and Thornton (2009) and a  $k_{14}/k_{12}$  ratio of 1 (i.e., both  $k_{12}$  and  $k_{14}$  are near the diffusion limit). This method largely follows the work of Ryder et al. (2015) who required a molar ratio of at least 2 to explain their observed  $\phi(\text{ClNO}_2)$  values on ambient sea water samples, assuming  $k_{14}/k_{12} = 1$ . The ratio required here to reproduce WINTER data ranged from 0 to  $>100$ , with a median of 6.0 and 4.2 for calculations with PILS and AMS chloride, respectively. For comparison, the median molar ratios

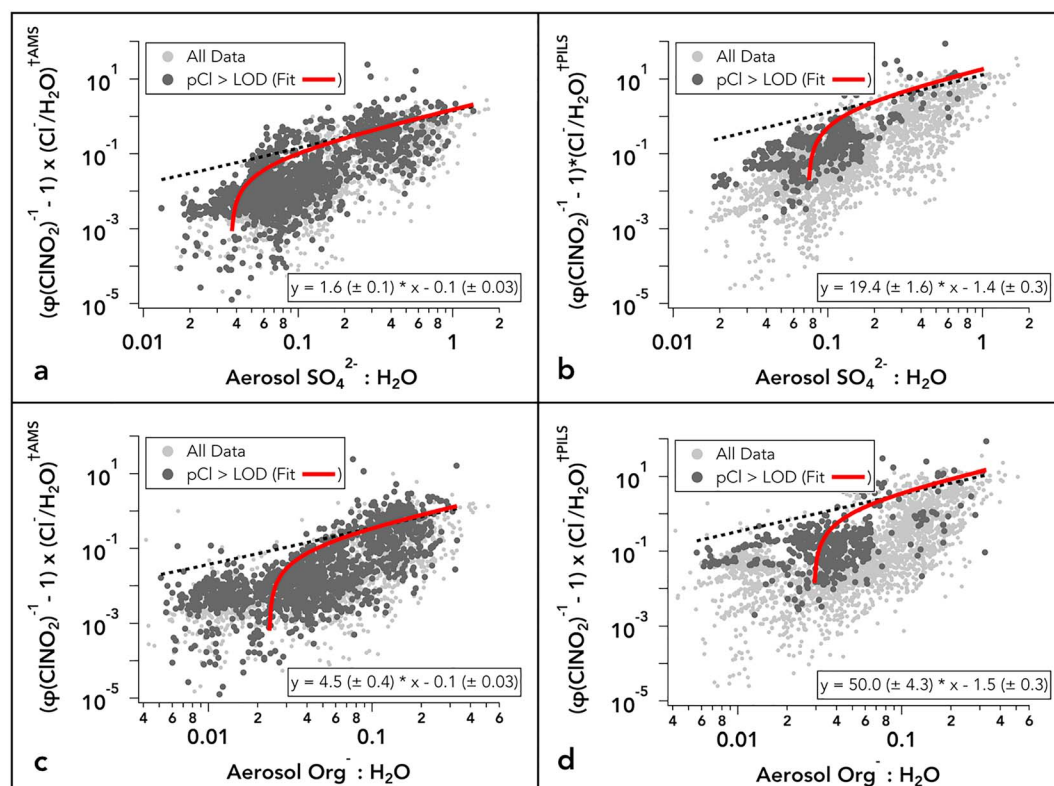


**Figure 7.** Correlation of the  $(\phi(\text{CINO}_2)^{-1} - 1) \times [\text{Cl}^-]/[\text{H}_2\text{O}]$  product from (7) (using box model  $\phi(\text{CINO}_2)$ ) against aerosol the  $\text{SO}_4^{2-}:\text{H}_2\text{O}$  molar ratio in panels (a) and (b) and Org: $\text{H}_2\text{O}$  molar ratio in panels (c) and (d), calculated using AMS (a and c) and PILS (b and d) chloride measurements. Points with corresponding particulate chloride above instrument detection limits are shown in dark gray. Red lines are the linear fits for each correlation with fit equation provided in each figure. Slopes represent the  $k_{14}/k_{12}$  ratio and intercepts represent the  $k_{11}/k_{12}$  ratio. Dashed lines represent the same fits, holding the intercept constant at 0.002 (from Bertram & Thornton, 2009). Organic molarity was calculated by applying a constant molecular weight of 250 g/mol to AMS organic mass concentration measurements. Larger y values correspond to smaller values of box model  $\phi(\text{CINO}_2)$ .

of  $\text{SO}_4^{2-}:\text{Cl}^-$  and  $\text{Org}^+:\text{Cl}^-$  during WINTER were between 7–25 and 2–11, respectively, but also with values exceeding 100.

Results in this section provide mixed evidence for the presence of a competition reaction between  $\text{Cl}^-$  and an additional reactive compound. The positive correlations between  $(\phi(\text{CINO}_2)^{-1} - 1) \times [\text{Cl}^-]/[\text{H}_2\text{O}]$  and molar ratios of  $\text{SO}_4^{2-}:\text{H}_2\text{O}$  and  $\text{Org}:\text{H}_2\text{O}$  are consistent with such reactions, but the intercepts that do not reproduce  $k_{11}/k_{12}$  in (7) suggest either that the model is incorrect for sulfate and organics or that there are multiple reactions and/or additional processes contributing to the observed  $\phi(\text{CINO}_2)$  suppression. Taking the  $k_{14}/k_{12}$  ratio in (7) as 1, the nucleophile in question would require molar ratios in excess of 100 relative to  $\text{Cl}^-$  to explain the lowest  $\phi(\text{CINO}_2)$  values. Many of the box model  $\phi(\text{CINO}_2)$  values, however, could be reproduced with much more moderate molar ratios of  $\sim 6$ . Further laboratory studies focused on the aqueous kinetics of  $\text{H}_2\text{ONO}_2^+$  will be required to assess the extent to which a process such as this explains the difference between observed and parameterized  $\phi(\text{CINO}_2)$  values.

#### 4.3.3. Direct $\text{CINO}_2$ Loss

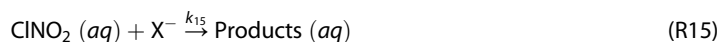
Lastly, direct loss of gas-phase  $\text{CINO}_2$  could additionally reduce modeled  $\phi(\text{CINO}_2)$  values relative to the parameterization. In the box model calculation of  $\phi(\text{CINO}_2)$ , values were derived by iteratively fitting the model output to gas-phase observations of  $\text{N}_2\text{O}_5$  and  $\text{CINO}_2$ . This method is based on the assumption that  $\text{CINO}_2$  formed from reaction (R12) will efficiently evaporate to the gas-phase based on the low solubility of  $\text{CINO}_2$  in water ( $K_H = 4 \times 10^{-2}$  M/atm; e.g., Frenzel et al., 1998; Roberts et al., 2008), where it is stable throughout the night. Additional direct loss mechanisms of  $\text{CINO}_2$ , independent from  $\text{N}_2\text{O}_5$ , would therefore serve to reduce the net  $\phi(\text{CINO}_2)$  derived by the model. Possible direct loss mechanisms could include: (1) gas-



phase  $\text{ClONO}_2$  loss through surface deposition and/or aerosol uptake and (2) direct aqueous-phase reaction of  $\text{ClONO}_2$  prior to evaporation.

Surface deposition and/or aerosol uptake of  $\text{ClONO}_2$  would serve to reduce the box model calculated  $\phi(\text{ClONO}_2)$  by reducing ambient gas-phase  $\text{ClONO}_2$  and the subsequently-derived  $\text{ClONO}_2$  production rate constant ( $k_{\text{ClONO}_2}$ ). The effect of  $\text{ClONO}_2$  loss from aerosol uptake is expected to be small as uptake coefficients have been measured on the order of  $1 \times 10^{-5}$  for dilute salt solutions (e.g., Frenzel et al., 1998; Schweitzer et al., 1998). Adjusting the box model-derived  $k_{\text{ClONO}_2}$  values in (1) for loss associated with an uptake coefficient of this magnitude increased the median box model  $\phi(\text{ClONO}_2)$  value by 1%. The potential loss of  $\text{ClONO}_2$  through ocean surface deposition has been discussed previously in sections 2.2 and S2.2.1. Though box model simulations were limited to the RL, increased mixed-layer depths over the ocean allow for possible air-sea exchange of  $\text{N}_2\text{O}_5$  and  $\text{ClONO}_2$  on WINTER flights over marine environments (Figure 1). While ocean emission of  $\text{ClONO}_2$  may be expected based on the positive water dependence of  $\text{N}_2\text{O}_5$  uptake (McDuffie et al., 2018, and references therein) and typical ocean salinity ( $\sim 0.55 \text{ M } [\text{Cl}^-]$ ), previous observations of  $\text{N}_2\text{O}_5$  and  $\text{ClONO}_2$  from the Scripps Institution of Oceanography (SIO) pier by Kim et al. (2014) found a net depositional flux of both  $\text{N}_2\text{O}_5$  and  $\text{ClONO}_2$  to the ocean surface. As previously discussed in section 2.2, adjusting the box model ( $k_{\text{N}_2\text{O}_5}$  and  $k_{\text{ClONO}_2}$ ) results for deposition of both  $\text{N}_2\text{O}_5$  and  $\text{ClONO}_2$  could reduce, but not entirely eliminate the difference between the  $\phi(\text{ClONO}_2)$  parameterization and box model results (Figure S3). Combined, these results suggest that possible gas-phase  $\text{ClONO}_2$  loss through aerosol uptake and/or ocean surface deposition may contribute to the low box model  $\phi(\text{ClONO}_2)$  values, but are not the only cause.

Direct loss of aqueous-phase  $\text{ClONO}_2$  could also reduce the box model  $\phi(\text{ClONO}_2)$  values relative to the simple parameterization. This could occur through direct aqueous-phase reaction of  $\text{ClONO}_2$  (aq) with species  $\text{X}^-$ , as generalized in reaction (R15). Though difficult to directly probe with WINTER field data, the possibility of direct  $\text{ClONO}_2$  reaction can be evaluated using the potential reaction products from (R15) and associated variables. For example, previous laboratory studies have identified reaction mechanisms for R15 that form halogenated products such as  $\text{Br}_2$ ,  $\text{BrNO}_2$  (Fickert et al., 1998; Frenzel et al., 1998; Schweitzer et al., 1998, 1999), or  $\text{Cl}_2$ , the latter of which is facilitated by particle acidity (Roberts et al., 2008). Three previous field studies with co-located  $\text{ClONO}_2$  and  $\text{Cl}_2$  observations from Colorado, California, and Calgary, however, did not consider heterogeneous  $\text{ClONO}_2$  chemistry a significant source of  $\text{Cl}_2$  due to weak ambient particle acidity (Mielke et al., 2011; Riedel et al., 2012, 2013). I-ToF-CIMS observations of  $\text{BrNO}_2$  did not exceed the instrument detection limit during WINTER (1 s,  $1\sigma$  of 1 pptv) and no statistically significant correlations were found between WINTER  $\phi(\text{ClONO}_2)$  values and I-ToF-CIMS observations of  $\text{Br}_2$  or  $\text{Cl}_2$  (above their 1 s,  $1\sigma$  detection limits of 0.5 and 0.4 pptv, respectively). In addition, a negative correlation ( $p < 0.05$ ) was observed between particle acidity and  $\text{Cl}_2$ , opposite of the expected trend from Roberts et al. (2008), despite high acidity calculated for aerosol during WINTER ( $\text{pH} \sim -2$  to 3; Guo et al., 2016).



Without further knowledge of the identity of species  $\text{X}^-$  and/or possible reaction products, the possibility of (R15) can be evaluated using the  $\phi(\text{ClONO}_2)$  expression in (8), derived from reactions (R9)–(R12) and (R15), assuming  $\text{H}_2\text{ONO}_2^+$  is in steady state, and that aqueous-phase  $\text{ClONO}_2$  is lost via (R15) before it can partition to the gas-phase via (R13) (derivation in section S4). Using (8), the  $k_{15}[\text{X}^-]$  ( $\text{s}^{-1}$ ) product required to reproduce box model  $\phi(\text{ClONO}_2)$  values was calculated for each point using values of  $\frac{k_{11}}{k_{12}}$  (0.002),  $\frac{k_{12}}{k_{10}}$  (29), and  $k'_9$  expression (defined in section S4) from Bertram and Thornton (2009), along with estimates of aqueous-phase concentrations of  $\text{N}_2\text{O}_5$  and  $\text{ClONO}_2$  from measured gas-phase mixing ratios and Henry's Law constants of 51 (unitless) (Fried et al., 1994) and  $4 \times 10^{-2} \text{ M/atm}$  (Frenzel et al., 1998; Roberts et al., 2008), respectively. Derived  $k_{15}[\text{X}^-]$  values suggest that reproduction of the box model values by invoking direct  $\text{ClONO}_2$  loss in (8) would require  $k_{15}[\text{X}^-]$  products between  $1 \times 10^5$  and  $8 \times 10^9 \text{ s}^{-1}$  for both AMS and PILS chloride. Assuming a larger solubility for  $\text{N}_2\text{O}_5$  of 5 M/atm (e.g., Griffiths et al., 2009; Mentel et al., 1999) would require even larger values of  $k_{15}[\text{X}^-]$ . Based on these results, the largest difference between the  $\phi(\text{ClONO}_2)$  parameterization and box model (requiring the largest  $k_{15}[\text{X}^-]$  value) would, therefore, require a reaction rate constant near the diffusion controlled limit ( $\sim 1 \times 10^9 \text{ M}^{-1} \text{ s}^{-1}$ ), or aqueous concentrations of  $[\text{X}^-]$  greater than 1 M. Median differences, however, could be reproduced with more moderate  $k_{15}[\text{X}^-]$  values of  $9 \times 10^7$  and  $1 \times 10^8 \text{ s}^{-1}$  for calculations with AMS and PILS chloride, respectively.

$$\phi(\text{ClNO}_2) = \frac{1}{\left(1 + \frac{k_{11}[\text{H}_2\text{O}]}{k_{12}[\text{Cl}^-]}\right)} - \frac{k_{15}[\text{X}^-][\text{ClNO}_2]_{\text{aq}}}{k'_9[\text{N}_2\text{O}_5]_{\text{aq}} \left(1 - \frac{1}{\frac{k_{11}[\text{H}_2\text{O}]}{k_{10}[\text{NO}_3^-]} + 1 + \frac{k_{12}[\text{Cl}^-]}{k_{10}[\text{NO}_3^-]}}\right)} \quad (8)$$

Results in this section are consistent with the possibility that direct loss of gas- and/or aqueous-phase  $\text{ClNO}_2$  could contribute to some of the smaller differences found in WINTER data between the  $\phi(\text{ClNO}_2)$  parameterization and box model. Agreement between these  $\phi(\text{ClNO}_2)$  values improved when considering the possibility of surface deposition of both gas-phase  $\text{ClNO}_2$  and  $\text{N}_2\text{O}_5$  (Figure S3), though box model median values remained lower than the parameterized equivalents. The addition of gas-phase loss through  $\text{ClNO}_2$  aerosol uptake only increased the median  $\phi(\text{ClNO}_2)$  by 1% when considering an uptake coefficient of  $1 \times 10^{-5}$ . The possible identity of species  $\text{X}^-$  in (R15) remains unknown. Low di-halogen concentrations do not provide evidence of direct loss through reactions with halogens, despite the highly acidic WINTER aerosol. Results from calculating  $k_{15}[\text{X}^-]$  in (8) suggest that direct aqueous loss of  $\text{ClNO}_2$  via (R15) would require concentrations of species  $[\text{X}^-] > 1 \text{ M}$  and/or reaction rate constants near the diffusion-limited rate to reproduce the lowest box model  $\phi(\text{ClNO}_2)$  values. Alternatively, in the event that  $\text{ClNO}_2$  were to remain unreacted and/or trapped in the aerosol due to an organic coating or changes in solubility, the box model  $\phi(\text{ClNO}_2)$  values would also appear lower than the parameterization. The cause of a physical trapping mechanism is uncertain, however, and if not water dependent, was not elucidated by correlations between  $\phi(\text{ClNO}_2)$  differences and aerosol composition (Table S3). In addition, any trapped  $\text{ClNO}_2$  would be reported as particle chloride by the AMS and would require 88% of the measured chloride to be from trapped aqueous-phase  $\text{ClNO}_2$  in order to account for the difference between the median box model and parameterized  $\phi(\text{ClNO}_2)$  values. Without additional information about WINTER aerosol composition, morphology/viscosity, and/or other possible aqueous-phase  $\text{ClNO}_2$  reactions, the possibility of direct aqueous-phase  $\text{ClNO}_2$  loss during WINTER cannot be further evaluated.

## 5. Conclusions

A box model analysis of 9 night flights during the 2015 WINTER aircraft campaign derived 3,425 individual determinations of  $\phi(\text{ClNO}_2)$  with a median value of 0.138 ( $1\sigma$ : +0.050/−0.045) and a range from 0.003 to 1. Comparison of a subset of WINTER box model  $\phi(\text{ClNO}_2)$  values to those calculated with two other commonly used, data-based methods, showed agreement between their predicted median values, within the uncertainty of each method. In contrast,  $\phi(\text{ClNO}_2)$  values calculated from a laboratory-based parameterization predicted a median value over a factor of two larger than all other methods and outside the bounds of the combined uncertainties for two. When compared to all WINTER data, the  $\phi(\text{ClNO}_2)$  parameterization over-predicted  $\geq 90\%$  of the box model values for points both above and below instrument detection limits for particulate chloride. In addition, the box model median  $\phi(\text{ClNO}_2)$  value was 75–84% lower than the median calculated with the Bertram and Thornton (2009) parameterization, using both AMS and PILS particulate chloride measurements. When considering the combined uncertainties associated with aerosol chloride and water concentrations, the lower-limit estimates of the  $\phi(\text{ClNO}_2)$  parameterization remained larger than 73% of the box model results. Similarly, upper-limit estimates of the box model results could not reconcile the differences between the box model and current  $\phi(\text{ClNO}_2)$  parameterization. These results are qualitatively consistent with all previous studies that have compared field-derived and parameterization-predicted  $\phi(\text{ClNO}_2)$  values.

Physiochemical processes related to this observed difference were assessed using ambient observations of aerosol composition and mechanistic processes that have been discussed in previous laboratory and field-based literature. The observed difference between parameterized and box-modeled  $\phi(\text{ClNO}_2)$  values was most strongly correlated with calculated aerosol water, with differences decreasing with increases in aerosol water molarity, liquid water content, and RH. This trend was caused by the opposite water dependences predicted by the  $\phi(\text{ClNO}_2)$  parameterization (negative) and the box model results (positive) and was not driven by uncertainties in the aerosol water calculation. A positive correlation between aerosol water and  $\phi(\text{ClNO}_2)$  has only been reported in one other field study and may be related to the physical availability of chloride, though this hypothesis could not be confirmed with WINTER data. In addition, the relatively low

correlation coefficients between  $\phi(\text{ClNO}_2)$  differences and aerosol water ( $\leq 0.53$ ) indicate that multiple factors may cause the low box model values relative to parameterized results.

WINTER results are consistent with additional mechanistic processes contributing to the field-parameterized  $\phi(\text{ClNO}_2)$  differences, except for those associated with the lowest water concentrations where the greatest differences were observed. These mechanistic processes include aqueous-/gas-phase  $\text{ClNO}_2$  loss and/or competition reactions with additional reactive aerosol components and were tested by deriving updated expressions for  $\phi(\text{ClNO}_2)$  after appending additional reactions to the original aqueous-phase formation mechanism. By invoking an additional competition reaction between  $\text{Cl}^-$  and an aqueous-phase compound [ $\text{Y}^-$ ], the  $\text{Y}^-/\text{Cl}^-$  molar ratio would need to be  $\sim 6$  to explain many of the differences between parameterized and box model-derived  $\phi(\text{ClNO}_2)$  values, with the largest differences requiring ratios  $>100$ . Tests setting  $\text{Y}^-$  to equal either  $\text{SO}_4^{2-}$  or total organics suggested that these particular species were not in direct competition with  $\text{Cl}^-$  via the applied model, or that there were multiple, overlapping processes leading to the observed  $\phi(\text{ClNO}_2)$  differences during WINTER. Similarly, loss of aqueous-phase  $\text{ClNO}_2$  by direct reaction with compound  $\text{X}^-$  could only reconcile the largest differences with a reaction rate constant near the diffusion limit or concentration of  $\text{X}^-$  greater than 1 M. In addition, loss of gas-phase  $\text{ClNO}_2$  through surface deposition or aerosol uptake could not explain the largest  $\phi(\text{ClNO}_2)$  differences. While WINTER data and box modeling results have provided valuable insights, further identification of mechanistic factors influencing  $\text{ClNO}_2$  formation will be required to develop a robust parameterization that can help improve model predictions of  $\text{ClNO}_2$  formation from  $\text{N}_2\text{O}_5$  heterogeneous uptake and lead to a better understanding of the halogen influence on tropospheric chemistry.

#### Acknowledgments

The authors would like to thank the NSF-NCAR Research Aircraft Facility staff. We also thank Rebecca S. Hornbrook, Eric C. Apel, and Alan J. Hills for TOGA VOC data from the WINTER campaign and comments during the manuscript preparation process. We finally thank Viral Shah for insightful discussions that informed this analysis. E. E. M. and S. S. B. acknowledge support from the NOAA Atmospheric Chemistry, Climate and Carbon Cycle (AC4) Program. Funding for D.L.F. was supported by NSF award 1433358. J.A.T. and the University of Washington group was funded by NSF AGS award 1360745. J. C. S., P. C. J., and J. L. J. acknowledge grants NSF AGS award 1360834 and NASA NNX15AT96G. The National Center for Atmospheric Research (NCAR) is sponsored by the National Science Foundation (NSF). J. D. was supported by NSF AGS award 1456249. All data from the WINTER campaign are available at [http://data.eol.ucar.edu/master\\_list/?project=WINTER](http://data.eol.ucar.edu/master_list/?project=WINTER). All referenced supplemental text, figures, and tables can be found in the supporting information. Code for the iterative box model can be found at <https://esrl.noaa.gov/csd/groups/csd7/measurements/2015winter/pubs/>.

#### References

- Anttila, T., Kiendler-Scharr, A., Tillmann, R., & Mentel, T. F. (2006). On the reactive uptake of gaseous compounds by organic-coated aqueous aerosols: Theoretical analysis and application to the heterogeneous hydrolysis of  $\text{N}_2\text{O}_5$ . *The Journal of Physical Chemistry A*, 110(35), 10,435–10,443. <https://doi.org/10.1021/jp062403c>
- Ault, A. P., Moffet, R. C., Baltrusaitis, J., Collins, D. B., Ruppel, M. J., Cuadra-Rodriguez, L. A., et al. (2013). Size-dependent changes in sea spray aerosol composition and properties with different seawater conditions. *Environmental Science & Technology*, 47(11), 5603–5612. <https://doi.org/10.1021/es400416g>
- Bannan, T. J., Bacak, A., le Breton, M., Flynn, M., Ouyang, B., McLeod, M., et al. (2017). Ground and airborne U.K. measurements of nitryl chloride: An investigation of the role of Cl atom oxidation at Weybourne atmospheric observatory. *Journal of Geophysical Research: Atmospheres*, 122, 11,154–11,165. <https://doi.org/10.1002/2017JD026624>
- Bannan, T. J., Booth, A. M., Bacak, A., Muller, J. B. A., Leather, K. E., le Breton, M., et al. (2015). The first UK measurements of nitryl chloride using a chemical ionization mass spectrometer in central London in the summer of 2012, and an investigation of the role of Cl atom oxidation. *Journal of Geophysical Research: Atmospheres*, 120, 5638–5657. <https://doi.org/10.1002/2014JD022629>
- Behnke, W., George, C., Scheer, V., & Zetzsch, C. (1997). Production and decay of  $\text{ClNO}_2$  from the reaction of gaseous  $\text{N}_2\text{O}_5$  with NaCl solution: Bulk and aerosol experiments. *Journal of Geophysical Research*, 102(D3), 3795–3804. <https://doi.org/10.1029/96JD03057>
- Behnke, W., Scheer, V., & Zetzsch, C. (1994). Production of  $\text{BrNO}_2$ ,  $\text{BrNO}$  and  $\text{ClNO}_2$  from the reaction between sea spray aerosol and  $\text{N}_2\text{O}_5$ . *Journal of Aerosol Science*, 25, 277–278. [https://doi.org/10.1016/0021-8502\(94\)90369-7](https://doi.org/10.1016/0021-8502(94)90369-7)
- Bertram, A. K., Martin, S. T., Hanna, S. J., Smith, M. L., Bodsworth, A., Chen, Q., et al. (2011). Predicting the relative humidities of liquid-liquid phase separation, efflorescence, and deliquescence of mixed particles of ammonium sulfate, organic material, and water using the organic-to-sulfate mass ratio of the particle and the oxygen-to-carbon elemental ratio of the organic component. *Atmospheric Chemistry and Physics*, 11(21), 10,995–11,006. <https://doi.org/10.5194/acp-11-10995-2011>
- Bertram, T. H., & Thornton, J. A. (2009). Toward a general parameterization of  $\text{N}_2\text{O}_5$  reactivity on aqueous particles: The competing effects of particle liquid water, nitrate and chloride. *Atmospheric Chemistry and Physics*, 9(21), 8351–8363. <https://doi.org/10.5194/acp-9-8351-2009>
- Brown, S. S., Dubé, W. P., Osthoff, H. D., Stutz, J., Ryerson, T. B., Wollny, A. G., et al. (2007). Vertical profiles in  $\text{NO}_3$  and  $\text{N}_2\text{O}_5$  measured from an aircraft: Results from the NOAA P-3 and surface platforms during the New England Air Quality Study 2004. *Journal of Geophysical Research*, 112, D22304. <https://doi.org/10.1029/2007JD008883>
- Brown, S. S., Stark, H., & Ravishankara, A. R. (2003). Applicability of the steady state approximation to the interpretation of atmospheric observations of  $\text{NO}_3$  and  $\text{N}_2\text{O}_5$ . *Journal of Geophysical Research*, 108(D17), 4539. <https://doi.org/10.1029/2003JD003407>
- Cummings, O. T., & Wick, C. D. (2013). Interfacial behavior of simple inorganic salts at the air-water interface investigated with a polarizable model with electrostatic damping. *The Journal of Chemical Physics*, 139(6), 064708. <https://doi.org/10.1063/1.4817775>
- Day, D. A., Wooldridge, P. J., Dillon, M. B., Thornton, J. A., & Cohen, R. C. (2002). A thermal dissociation laser-induced fluorescence instrument for in situ detection of  $\text{NO}_2$ , peroxy nitrates, alkyl nitrates, and  $\text{HNO}_3$ . *Journal of Geophysical Research*, 107(D6), 4046. <https://doi.org/10.1029/2001JD000779>
- DeCarlo, P. F., Kimmel, J. R., Trimborn, A., Northway, M. J., Jayne, J. T., Aiken, A. C., et al. (2006). Field-deployable, high-resolution, time-of-flight aerosol mass spectrometer. *Analytical Chemistry*, 78(24), 8281–8289. <https://doi.org/10.1021/ac061249n>
- Dubé, W. P., Brown, S. S., Osthoff, H. D., Nunley, M. R., Ciciora, S. J., Paris, M. W., et al. (2006). Aircraft instrument for simultaneous, in situ measurement of  $\text{NO}_3$  and  $\text{N}_2\text{O}_5$  via pulsed cavity ring-down spectroscopy. *Review of Scientific Instruments*, 77(3), 034101. <https://doi.org/10.1063/1.2176058>
- Edwards, P. M., Young, C. J., Aikin, K., deGouw, J., Dubé, W. P., Geiger, F., et al. (2013). Ozone photochemistry in an oil and natural gas extraction region during winter: Simulations of a snow-free season in the Uintah Basin, Utah. *Atmospheric Chemistry and Physics*, 13(17), 8955–8971. <https://doi.org/10.5194/acp-13-8955-2013>

- Faxon, C. B., Bean, J. K., & Ruiz, L. H. (2015). Inland concentrations of  $\text{Cl}_2$  and  $\text{ClNO}_2$  in southeast Texas suggest chlorine chemistry significantly contributes to atmospheric reactivity. *Atmosphere*, 6(10), 1487–1506. <https://doi.org/10.3390/atmos6101487>
- Fibiger, D. L., McDuffie, E. E., Dubé, W. P., Aikin, K. C., Lopez-Hilfiker, F. D., Lee, B. H., et al. (2018). Wintertime overnight  $\text{NO}_x$  removal in a southeastern United States coal-fired power plant plume: A model for understanding winter  $\text{NO}_x$  processing and its implications. *Journal of Geophysical Research: Atmospheres*, 123, 1412–1425. <https://doi.org/10.1002/2017JD027768>
- Fickert, S., Helleis, F., Adams, J. W., Moortgat, G. K., & Crowley, J. N. (1998). Reactive uptake of  $\text{ClNO}_2$  on aqueous bromide solutions. *Journal of Physical Chemistry A*, 102(52), 10,689–10,696. <https://doi.org/10.1021/jp983004n>
- Fountoukis, C., & Nenes, A. (2007). ISORROPIA II: A computationally efficient thermodynamic equilibrium model for  $\text{K}^+$ - $\text{Ca}^{2+}$ - $\text{Mg}^{2+}$ - $\text{NH}_4^+$ - $\text{Na}^+$ - $\text{SO}_4^{2-}$ - $\text{NO}_3^-$ - $\text{Cl}^-$ - $\text{H}_2\text{O}$  aerosols. *Atmospheric Chemistry and Physics*, 7(17), 4639–4659. <https://doi.org/10.5194/acp-7-4639-2007>
- Frenzel, A., Scheer, V., Sikorski, R., George, C., Behnke, W., & Zetzsch, C. (1998). Heterogeneous interconversion reactions of  $\text{BrNO}_2$ ,  $\text{ClNO}_2$ ,  $\text{Br}_2$ , and  $\text{Cl}_2$ . *The Journal of Physical Chemistry A*, 102(8), 1329–1337. <https://doi.org/10.1021/jp973044b>
- Fried, A., Henry, B. E., Calvert, J. G., & Mozurkewich, M. (1994). The reaction probability of  $\text{N}_2\text{O}_5$  with sulfuric acid aerosols at stratospheric temperatures and compositions. *Journal of Geophysical Research*, 99(D2), 3517–3532. <https://doi.org/10.1029/93JD01907>
- Fuchs, H., Dube, W. P., Lerner, B. M., Wagner, N. L., Williams, E. J., & Brown, S. S. (2009). A sensitive and versatile detector for atmospheric  $\text{NO}_2$  and  $\text{NO}_x$  based on blue diode laser cavity ring-down spectroscopy. *Environmental Science & Technology*, 43(20), 7831–7836. <https://doi.org/10.1021/es902067h>
- Gaston, C. J., & Thornton, J. A. (2016). Reacto-diffusive length of  $\text{N}_2\text{O}_5$  in aqueous sulfate- and chloride-containing aerosol particles. *Journal of Physical Chemistry A*, 120(7), 1039–1045. <https://doi.org/10.1021/acs.jpca.5b11914>
- Gaston, C. J., Thornton, J. A., & Ng, N. L. (2014). Reactive uptake of  $\text{N}_2\text{O}_5$  to internally mixed inorganic and organic particles: The role of organic carbon oxidation state and inferred organic phase separations. *Atmospheric Chemistry and Physics*, 14(11), 5693–5707. <https://doi.org/10.5194/acp-14-5693-2014>
- Griffiths, P. T., Badger, C. L., Cox, R. A., Folkers, M., Henk, H. H., & Mentel, T. F. (2009). Reactive uptake of  $\text{N}_2\text{O}_5$  by aerosols containing dicarboxylic acids. Effect of particle phase, composition, and nitrate content. *The Journal of Physical Chemistry A*, 113(17), 5082–5090. <https://doi.org/10.1021/jp8096814>
- Gržinić, G., Bartels-Rausch, T., Berkemeier, T., Türlér, A., & Ammann, M. (2015). Viscosity controls humidity dependence of  $\text{N}_2\text{O}_5$  uptake to citric acid aerosol. *Atmospheric Chemistry and Physics*, 15(23), 13,615–13,625. <https://doi.org/10.5194/acp-15-13615-2015>
- Guo, H., Sullivan, A. P., Campuzano-Jost, P., Schroder, J. C., Lopez-Hilfiker, F. D., Dibb, J. E., et al. (2016). Fine particle pH and the partitioning of nitric acid during winter in the northeastern United States. *Journal of Geophysical Research: Atmospheres*, 121, 10,355–10,376. <https://doi.org/10.1002/2016JD025311>
- Hayes, P. L., Ortega, A. M., Cubison, M. J., Froyd, K. D., Zhao, Y., Cliff, S. S., et al. (2013). Organic aerosol composition and sources in Pasadena, California, during the 2010 CalNex campaign. *Journal of Geophysical Research: Atmospheres*, 118, 9233–9257. <https://doi.org/10.1002/jgrd.50530>
- Heal, M. R., Harrison, M. A. J., & Neil Cape, J. (2007). Aqueous-phase nitration of phenol by  $\text{N}_2\text{O}_5$  and  $\text{ClNO}_2$ . *Atmospheric Environment*, 41(17), 3515–3520. <https://doi.org/10.1016/j.atmosenv.2007.02.003>
- Hoggett, J. G., Moodie, R. B., Penton, J. R., & Schofield, K. (1971). *Nitration and aromatic reactivity*. Great Britain: Univ. Press.
- Kenagy, H. S., Sparks, T. L., Ebben, C. J., Wooldridge, P. J., Lopez-Hilfiker, F. D., Lee, B. H., et al. (2018).  $\text{NO}_x$  lifetime and  $\text{NO}_y$  partitioning during WINTER. *Journal of Geophysical Research: Atmospheres*, 123, 9813–9827. <https://doi.org/10.1029/2018JD028736>
- Kercher, J. P., Riedel, T. P., & Thornton, J. A. (2009). Chlorine activation by  $\text{N}_2\text{O}_5$ : Simultaneous, in situ detection of  $\text{ClNO}_2$  and  $\text{N}_2\text{O}_5$  by chemical ionization mass spectrometry. *Atmospheric Measurement Techniques*, 2(1), 193–204. <https://doi.org/10.5194/amt-2-193-2009>
- Kim, M. J., Farmer, D. K., & Bertram, T. H. (2014). A controlling role for the air–sea interface in the chemical processing of reactive nitrogen in the coastal marine boundary layer. *Proceedings of the National Academy of Sciences of the United States of America*, 111(11), 3943–3948. <https://doi.org/10.1073/pnas.1318694111>
- Laskin, A., Moffet, R. C., Gilles, M. K., Fast, J. D., Zaveri, R. A., Wang, B., et al. (2012). Tropospheric chemistry of internally mixed sea salt and organic particles: Surprising reactivity of  $\text{NaCl}$  with weak organic acids. *Journal of Geophysical Research*, 117, D15302. <https://doi.org/10.1029/2012JD017743>
- Lee, B. H., Lopez-Hilfiker, F. D., Mohr, C., Kurtén, T., Worsnop, D. R., & Thornton, J. A. (2014). An iodide-adduct high-resolution time-of-flight chemical-ionization mass spectrometer: Application to atmospheric inorganic and organic compounds. *Environmental Science & Technology*, 48(11), 6309–6317. <https://doi.org/10.1021/es500362a>
- Lee, B. H., Lopez-Hilfiker, F. D., Schroder, J. C., Campuzano-Jost, P., Jimenez, J. L., McDuffie, E. E., et al. (2018). Airborne observations of reactive inorganic chlorine and bromine species in the exhaust of coal-fired power plants. *Journal of Geophysical Research: Atmospheres*. <https://doi.org/10.1029/2018JD029284>, 123, 11,225–11,237.
- Liu, X., Qu, H., Huey, L. G., Wang, Y., Sjostedt, S., Zeng, L., et al. (2017). High levels of daytime molecular chlorine and nitryl chloride at a rural site on the North China Plain. *Environmental Science & Technology*, 51(17), 9588–9595. <https://doi.org/10.1021/acs.est.7b03039>
- Lopez-Hilfiker, F. D., Constantin, K., Kercher, J. P., & Thornton, J. A. (2012). Temperature dependent halogen activation by  $\text{N}_2\text{O}_5$  reactions on halide-doped ice surfaces. *Atmospheric Chemistry and Physics*, 12(11), 5237–5247. <https://doi.org/10.5194/acp-12-5237-2012>
- Lüttke, J., Scheer, V., Levens, K., Wünsch, G., Neil Cape, J., Hargreaves, K. J., Storeton-West, R. L., et al. (1997). Occurrence and formation of nitrated phenols in and out of cloud. *Atmospheric Environment*, 31(16), 2637–2648. [https://doi.org/10.1016/S1352-2310\(96\)00229-4](https://doi.org/10.1016/S1352-2310(96)00229-4)
- Maclean, A. M., Butenhoff, C. L., Grayson, J. W., Barsanti, K., Jimenez, J. L., & Bertram, A. K. (2017). Mixing times of organic molecules within secondary organic aerosol particles: A global planetary boundary layer perspective. *Atmospheric Chemistry and Physics*, 17(21), 13,037–13,048. <https://doi.org/10.5194/acp-17-13037-2017>
- Madronich, S. S., McKenzie, R. L., Bjorn, L. O., & Caldwell, M. M. (1998). Changes in biologically active ultraviolet radiation reaching the Earth's surface. *Journal of Photochemistry and Photobiology B: Biology*, 46(1–3), 5–19. [https://doi.org/10.1016/S1011-1344\(98\)00182-1](https://doi.org/10.1016/S1011-1344(98)00182-1)
- McDuffie, E. E., Fibiger, D. L., Dubé, W. P., Lopez-Hilfiker, F., Lee, B. H., Thornton, J. A., et al. (2018). Heterogeneous  $\text{N}_2\text{O}_5$  uptake during WINTER: Aircraft measurements during the 2015 WINTER campaign and critical evaluation of current parameterizations. *Journal of Geophysical Research: Atmospheres*, 123, 4345–4372. <https://doi.org/10.1002/2018JD028336>
- Mentel, T. F., Sohn, M., & Wahner, A. (1999). Nitrate effect in the heterogeneous hydrolysis of dinitrogen pentoxide on aqueous aerosols. *Physical Chemistry Chemical Physics*, 1(24), 5451–5457. <https://doi.org/10.1039/A905338G>
- Mielke, L. H., Furgeson, A., Odame-Ankrah, C. A., & Osthoff, H. D. (2016). Ubiquity of  $\text{ClNO}_2$  in the urban boundary layer of Calgary, Alberta, Canada. *Canadian Journal of Chemistry*, 94(4), 414–423. <https://doi.org/10.1139/cjc-2015-0426>
- Mielke, L. H., Furgeson, A., & Osthoff, H. D. (2011). Observation of  $\text{ClNO}_2$  in a mid-continental urban environment. *Environmental Science & Technology*, 45(20), 8889–8896. <https://doi.org/10.1021/es201955u>



- Mielke, L. H., Stutz, J., Tsai, C., Hurlock, S. C., Roberts, J. M., Veres, P. R., et al. (2013). Heterogeneous formation of nitryl chloride and its role as a nocturnal  $\text{NO}_x$  reservoir species during CalNex-LA 2010. *Journal of Geophysical Research: Atmospheres*, 118, 10,638–10,652. <https://doi.org/10.1002/jgrd.50783>
- Osthoff, H. D., Roberts, J. M., Ravishankara, A. R., Williams, E. J., Lerner, B. M., Sommariva, R., et al. (2008). High levels of nitryl chloride in the polluted subtropical marine boundary layer. *Nature Geoscience*, 1(5), 324–328. <https://doi.org/10.1038/ngeo177>
- Phillips, G. J., Tang, M. J., Thieser, J., Brickwedde, B., Schuster, G., Bohn, B., et al. (2012). Significant concentrations of nitryl chloride observed in rural continental Europe associated with the influence of sea salt chloride and anthropogenic emissions. *Geophysical Research Letters*, 39, L10811. <https://doi.org/10.1029/2012GL051912>
- Phillips, G. J., Thieser, J., Tang, M., Sobanski, N., Schuster, G., Fachinger, J., et al. (2016). Estimating  $\text{N}_2\text{O}_5$  uptake coefficients using ambient measurements of  $\text{NO}_3$ ,  $\text{N}_2\text{O}_5$ ,  $\text{ClNO}_2$  and particle-phase nitrate. *Atmospheric Chemistry and Physics*, 16(20), 13,231–13,249. <https://doi.org/10.5194/acp-16-13231-2016>
- Reyes-Villegas, E., Priestley, M., Ting, Y. C., Haslett, S., Bannan, T., le Breton, M., et al. (2018). Simultaneous aerosol mass spectrometry and chemical ionisation mass spectrometry measurements during a biomass burning event in the UK: Insights into nitrate chemistry. *Atmospheric Chemistry and Physics*, 18(6), 4093–4111. <https://doi.org/10.5194/acp-18-4093-2018>
- Riedel, T. P., Bertram, T. H., Crisp, T. A., Williams, E. J., Lerner, B. M., Vlasenko, A., et al. (2012). Nitryl chloride and molecular chlorine in the coastal marine boundary layer. *Environmental Science & Technology*, 46(19), 10,463–10,470. <https://doi.org/10.1021/es204632r>
- Riedel, T. P., Wagner, N. L., Dubé, W. P., Middlebrook, A. M., Young, C. J., Öztürk, F., et al. (2013). Chlorine activation within urban or power plant plumes: Vertically resolved  $\text{ClNO}_2$  and  $\text{Cl}_2$  measurements from a tall tower in a polluted continental setting. *Journal of Geophysical Research: Atmospheres*, 118, 8702–8715. <https://doi.org/10.1002/jgrd.50637>
- Roberts, J. M., Osthoff, H. D., Brown, S. S., & Ravishankara, A. R. (2008).  $\text{N}_2\text{O}_5$  oxidizes chloride to  $\text{Cl}_2$  in acidic atmospheric aerosol. *Science*, 321(5892), 1059. <https://doi.org/10.1126/science.1158777>
- Roberts, J. M., Osthoff, H. D., Brown, S. S., Ravishankara, A. R., Coffman, D., Quinn, P., & Bates, T. (2009). Laboratory studies of products of  $\text{N}_2\text{O}_5$  uptake on  $\text{Cl}^-$  containing substrates. *Geophysical Research Letters*, 36, L20808. <https://doi.org/10.1029/2009GL040448>
- Ryder, O. S., Campbell, N. R., Shalowski, M., Al-Mashat, H., Nathanson, G. M., & Bertram, T. H. (2015). Role of organics in regulating  $\text{ClNO}_2$  production at the air–sea interface. *The Journal of Physical Chemistry A*, 119(31), 8519–8526. <https://doi.org/10.1021/jp5129673>
- Sarwar, G., Simon, H., Xing, J., & Mathur, R. (2014). Importance of tropospheric  $\text{ClNO}_2$  chemistry across the Northern Hemisphere. *Geophysical Research Letters*, 41, 4050–4058. <https://doi.org/10.1002/2014gl059962>
- Schofield, K. (1980). *Aromatic nitration*. Great Britain: University Press.
- Schroder, J. C., Campuzano-Jost, P., Day, D. A., Shah, V., Larson, K., Sommers, J. M., et al. (2018). Sources and secondary production of organic aerosols in the northeastern US during WINTER. *Journal of Geophysical Research: Atmospheres*, 123, 7771–7796. <https://doi.org/10.1029/2018JD028475>
- Schweitzer, F., Mirabel, P., & George, C. (1998). Multiphase chemistry of  $\text{N}_2\text{O}_5$ ,  $\text{ClNO}_2$ , and  $\text{BrNO}_2$ . *The Journal of Physical Chemistry A*, 102(22), 3942–3952. <https://doi.org/10.1021/jp980748s>
- Schweitzer, F., Mirabel, P., & George, C. (1999). Heterogeneous chemistry of nitryl halides in relation to tropospheric halogen activation. *Journal of Atmospheric Chemistry*, 34(1), 101–117. <https://doi.org/10.1023/A:1006249921480>
- Seidel, D. J., Zhang, Y., Beljaars, A., Golaz, J.-C., Jacobson, A. R., & Medeiros, B. (2012). Climatology of the planetary boundary layer over the continental United States and Europe. *Journal of Geophysical Research*, 117, D17106. <https://doi.org/10.1029/2012JD018143>
- Sherwen, T., Evans, M. J., Sommariva, R., Hollis, L. D. J., Ball, S. M., Monks, P. S., Reed, C., et al. (2017). Effects of halogens on European air-quality. *Faraday Discussions*, 200, 75–100. <https://doi.org/10.1039/C7FD00026j>
- Shetter, R. E., & Müller, M. (1999). Photolysis frequency measurements using actinic flux spectroradiometry during the PEM-Tropics mission: Instrumentation description and some results. *Journal of Geophysical Research*, 104(D5), 5647–5661. <https://doi.org/10.1029/98JD01381>
- Shiraiwa, M., Li, Y., Tsimpidi, A. P., Karydis, V. A., Berkemeier, T., Pandis, S. N., et al. (2017). Global distribution of particle phase state in atmospheric secondary organic aerosols. *Nature Communications*, 8, 15002. <https://doi.org/10.1038/ncomms15002>
- Simpson, W. R., Brown, S. S., Saiz-Lopez, A., Thornton, J. A., & von Glasow, R. (2015). Tropospheric halogen chemistry: Sources, cycling, and impacts. *Chemical Reviews*, 115(10), 4035–4062. <https://doi.org/10.1021/cr5006638>
- Taylor, R. (1990). *Electrophillic aromatic substitution*. New York: John Wiley.
- Tham, Y. J., Wang, Z., Li, Q., Wang, W., Wang, X., Lu, K., Ma, N., et al. (2018). Heterogeneous  $\text{N}_2\text{O}_5$  uptake coefficient and production yield of  $\text{ClNO}_2$  in polluted northern China: Roles of aerosol water content and chemical composition. *Atmospheric Chemistry and Physics Discussions*, 2018, 1–27. <https://doi.org/10.5194/acp-2018-313>
- Tham, Y. J., Wang, Z., Li, Q., Yun, H., Wang, W., Wang, X., et al. (2016). Significant concentrations of nitryl chloride sustained in the morning: Investigations of the causes and impacts on ozone production in a polluted region of northern China. *Atmospheric Chemistry and Physics*, 16(23), 14,959–14,977. <https://doi.org/10.5194/acp-16-14959-2016>
- Tham, Y. J., Yan, C., Xue, L., Zha, Q., Wang, X., & Wang, T. (2014). Presence of high nitryl chloride in Asian coastal environment and its impact on atmospheric photochemistry. *Chinese Science Bulletin*, 59(4), 356–359. <https://doi.org/10.1007/s11434-013-0063-y>
- Thornton, J. A., Kercher, J. P., Riedel, T. P., Wagner, N. L., Cozic, J., Holloway, J. S., et al. (2010). A large atomic chlorine source inferred from mid-continental reactive nitrogen chemistry. *Nature*, 464(7286), 271–274. <https://doi.org/10.1038/nature08905>
- Wagner, N. L., Dubé, W. P., Washenfelder, R. A., Young, C. J., Pollack, I. B., Ryerson, T. B., & Brown, S. S. (2011). Diode laser-based cavity ring-down instrument for  $\text{NO}_3$ ,  $\text{N}_2\text{O}_5$ ,  $\text{NO}$ ,  $\text{NO}_2$  and  $\text{O}_3$  from aircraft. *Atmospheric Measurement Techniques*, 4(6), 1227–1240. <https://doi.org/10.5194/amt-4-1227-2011>
- Wagner, N. L., Riedel, T. P., Roberts, J. M., Thornton, J. A., Angevine, W. M., Williams, E. J., et al. (2012). The sea breeze/land breeze circulation in Los Angeles and its influence on nitryl chloride production in this region. *Journal of Geophysical Research*, 117, D00V24. <https://doi.org/10.1029/2012JD017810>
- Wagner, N. L., Riedel, T. P., Young, C. J., Bahreini, R., Brock, C. A., Dubé, W. P., et al. (2013).  $\text{N}_2\text{O}_5$  uptake coefficients and nocturnal  $\text{NO}_2$  removal rates determined from ambient wintertime measurements. *Journal of Geophysical Research: Atmospheres*, 118, 9331–9350. <https://doi.org/10.1002/jgrd.50653>
- Wang, H., Lu, K., Guo, S., Wu, Z., Shang, D., Tan, Z., et al. (2018). Efficient  $\text{N}_2\text{O}_5$  uptake and  $\text{NO}_3$  oxidation in the outflow of urban Beijing. *Atmospheric Chemistry and Physics Discussions*, 2018, 1–27. <https://doi.org/10.5194/acp-2018-88>
- Wang, T., Tham, Y. J., Xue, L., Li, Q., Zha, Q., Wang, Z., et al. (2016). Observations of nitryl chloride and modeling its source and effect on ozone in the planetary boundary layer of southern China. *Journal of Geophysical Research: Atmospheres*, 121, 2476–2489. <https://doi.org/10.1002/2015JD024556>

- Wang, X., Wang, H., Xue, L., Wang, T., Wang, L., Gu, R., et al. (2017). Observations of  $\text{N}_2\text{O}_5$  and  $\text{ClNO}_2$  at a polluted urban surface site in North China: High  $\text{N}_2\text{O}_5$  uptake coefficients and low  $\text{ClNO}_2$  product yields. *Atmospheric Environment*, 156, 125–134. <https://doi.org/10.1016/j.atmosenv.2017.02.035>
- Wang, X., Wang, T., Yan, C., Tham, Y. J., Xue, L., Xu, Z., & Zha, Q. (2014). Large daytime signals of  $\text{N}_2\text{O}_5$  and  $\text{NO}_3$  inferred at 62 amu in a TD-CIMS: Chemical interference or a real atmospheric phenomenon? *Atmospheric Measurement Techniques*, 7(1), 1–12. <https://doi.org/10.5194/amt-7-1-2014>
- Wang, Z., Wang, W., Tham, Y. J., Li, Q., Wang, H., Wen, L., et al. (2017). Fast heterogeneous  $\text{N}_2\text{O}_5$  uptake and  $\text{ClNO}_2$  production in power plant and industrial plumes observed in the nocturnal residual layer over the North China Plain. *Atmospheric Chemistry and Physics*, 17(20), 12,361–12,378. <https://doi.org/10.5194/acp-17-12361-2017>
- Washenfelder, R. A., Wagner, N. L., Dube, W. P., & Brown, S. S. (2011). Measurement of atmospheric ozone by cavity ring-down spectroscopy. *Environmental Science & Technology*, 45(7), 2938–2944. <https://doi.org/10.1021/es103340u>
- Weinheimer, A. J., Walega, J. G., Ridley, B. A., Gary, B. L., Blake, D. R., Blake, N. J., et al. (1994). Meridional distributions of  $\text{NO}_x$ ,  $\text{NO}_y$ , and other species in the lower stratosphere and upper troposphere during AASE II. *Geophysical Research Letters*, 21(23), 2583–2586. <https://doi.org/10.1029/94GL01897>
- Wild, R. J., Edwards, P. M., Bates, T. S., Cohen, R. C., de Gouw, J. A., Dubé, W. P., et al. (2016). Reactive nitrogen partitioning and its relationship to winter ozone events in Utah. *Atmospheric Chemistry and Physics*, 16(2), 573–583. <https://doi.org/10.5194/acp-16-573-2016>
- Young, A. H., Keene, W. C., Pszenny, A. A. P., Sander, R., Thornton, J. A., Riedel, T. P., & Maben, J. R. (2013). Phase partitioning of soluble trace gases with size-resolved aerosols in near-surface continental air over northern Colorado, USA, during winter. *Journal of Geophysical Research: Atmospheres*, 118, 9414–9427. <https://doi.org/10.1002/jgrd.50655>
- Young, C. J., Washenfelder, R. A., Roberts, J. M., Mielke, L. H., Osthoff, H. D., Tsai, C., et al. (2012). Vertically resolved measurements of nighttime radical reservoirs in Los Angeles and their contribution to the urban radical budget. *Environmental Science & Technology*, 46(20), 10,965–10,973. <https://doi.org/10.1021/es302206a>
- Yun, H., Wang, T., Wang, W., Tham, Y. J., Li, Q., Wang, Z., & Poon, S. C. N. (2018). Nighttime  $\text{NO}_x$  loss and  $\text{ClNO}_2$  formation in the residual layer of a polluted region: Insights from field measurements and an iterative box model. *Science of the Total Environment*, 622–623, 727–734. <https://doi.org/10.1016/j.scitotenv.2017.11.352>